NASA CONTRACTOR
REPORT

NASA CR-143876

(NASA-CR-143876) FLOAT ZONE PROCESSING IN A WEIGHTLESS ENVIRONMENT Summary Report (Little (Arthur D.), Inc.) 70 p HC $4.25 CSCL 22A

N75-27023

Unclas
G3/12 28014

FLAT ZONE PROCESSING IN A WEIGHTLESS ENVIRONMENT

By A. A. Fowle, J. S. Haggerty, P. F. Strong, G. Rudenberg, and R. Kronauer

Arthur D. Little, Inc.
Cambridge, Massachusetts 02140

October 1974

Summary Report

Prepared for

NASA-GEORGE C. MARSHALL SPACE FLIGHT CENTER
Marshall Space Flight Center, Alabama 35812

TECHNICAL REPORT STANDARD TITLE PAGE

1. REPORT NO.	2. GOVERNMENT ACCESSION NO.	3. RECIPIENT'S CATALOG NO.
NASA CR-143876		

4. TITLE AND SUBTITLE	5. REPORT DATE
Float Zone Processing in a Weightless Environment	October 1974
	6. PERFORMING ORGANIZATION CODE

7. AUTHOR(S)	8. PERFORMING ORGANIZATION REPORT #
A. A. Fowle, J. S. Haggerty, P. F. Strong, G. Rudenberg, and R. Kronauer	

9. PERFORMING ORGANIZATION NAME AND ADDRESS	10. WORK UNIT NO.
Arthur D. Little, Inc. Cambridge, Massachusetts 02140	11. CONTRACT OR GRANT NO. NAS8-29877

12. SPONSORING AGENCY NAME AND ADDRESS	13. TYPE OF REPORT & PERIOD COVERED
National Aeronautics and Space Administration Washington, D. C. 20546	Contractor, Summary
	14. SPONSORING AGENCY CODE

15. SUPPLEMENTARY NOTES

16. ABSTRACT

This report documents the results of investigations into: 1) the physical limits which set the maximum practical diameters of Si crystals that can be processed by the float-zone method in a near weightless environment, and 2) the economic impact of large, space-produced Si crystals on the electronics industry.

Areas of technological investigation focus on evaluations of the stability of the melt and heat transfer and fluid flow within the melt as dependent on the crystal size and the degree and type of rotation imparted to the melt—all in search of best methods for utilizing the weightless environment for the production of large, stress-free Si crystals of uniform composition.

The economic impact analysis consists of an evaluation of the effect of large size [up to 20 cm (7.8 inches) diameter] Si crystals, and on their potential applications, likely utilization and cost advantages in LSI, integrated circuits, and power devices. This relates to the foreseeable advantages of larger diameter wafers of good characteristics and the possibilities seen for greater perfection resulting from stress-free growth.

17. KEY WORDS	18. DISTRIBUTION STATEMENT
Crystal growth Float zone Space processing	Unclassified - Unlimited James A. Littleton for Mirt C. Davidson

19. SECURITY CLASSIF. (of this report)	20. SECURITY CLASSIF. (of this page)	21. NO. OF PAGES	22. PRICE
Unclassified	Unclassified	70	NTIS

FOREWORD

A summary report is presented on work performed during the period January to September 1974 on Contract NAS8-29877, "Float-Zone Processing in a Weightless Environment." The reported work set forth the results of evaluations to determine: 1) some practical limits on the size of Si crystals that can be grown in a Skylab-type space vehicle, and 2) the economic impact of large, space-produced Si crystals on the electronics industry.

This study program is sponsored by the George C. Marshall Space Flight Center, National Aeronautics and Space Administration, Huntsville, Alabama. Mr. M. Davidson is the COR director of the study. Dr. A. A. Fowle, Dr. J. S. Haggerty, Mr. P. F. Strong and Dr. G. Rudenberg of Arthur D. Little, Inc., and Prof. R. Kronauer of Harvard University are the investigators.

TABLE OF CONTENTS

TABLE OF CONTENTS (Cont'd)

LIST OF FIGURES

LIST OF TABLES

1.0 SUMMARY

1.1 PURPOSE AND SCOPE

The objective of this work is to evaluate and maximize the potential benefits of producing faultless silicon crystals in a space environment by the float-zone process. A perceived benefit is the possibility of producing larger diameter crystals than can be achieved on earth which may translate into less expensive crystal elements for final use. By incorporating relative rotation between the crystal and feed stock, forced convective currents may be induced in the melt which can result in a radial distribution of axial heat flux at the freezing interface which reduces grown-in stresses for crystals of the larger sizes that are possible to produce in the near zero gravity environment. Specifically the objectives of the program were:

1. Analyze the stability of floating zones to determine the practical diameters of Si crystals that can be processed in a near zero gravity environment. These diameters will be related to rotation rates based on estimates set by stability criteria.

2. For the diameters determined in (1), carry out an economic analysis to project the ten year impact to the electronics industry. This analysis will include the expected advantages on the individual manufacturing phases of integrated circuits.

1.2 CONCLUSIONS AND RECOMMENDATIONS

1.2.1 The Technology of Float-Zone Crystal Growing Process in Space

Stable molten zones in practical configurations for crystals as large as 0.304 m (12 inch) radius can be maintained with limited but useful rotation rates in a float-zone process in a near zero gravity environment.

The use of isorotation or counterrotation, rotational rates, and crystal and feed stock diameter ratios have been examined qualitatively and semi-quantitatively for their influence on producing stress-free crystals of uniform composition. Some tentative specification of these process variables for best results have been made; however, a combination of experimentation and more analysis is needed before a specification of these variables for improved and/or larger space grown crystals can be made with confidence.

As a first priority, we recommend some experiments based on model studies in order to provide further information relating to the stability of and circulation within the molten zone of a silicon crystal process in space. The control of fluid motion within the molten zone is critical to a

successful process and, therefore, a complete understanding of this motion is necessary to any further, useful analyses directed to the optimization of the process. These experiments are recommended as the most effective next step in a program leading to the design of a space experiment.

1.2.2 Economic Impact

There is considerable value in large diameter uniform crystals and wafers for the electronics industry. This is already evident by the shift from 5 cm (2 inch) to 7.6 cm (3 inch) diameter crystals by the industry. The present study shows that a number of applications can be identified where much larger wafers with uniform characteristics have commercial value. The principal value of the large wafers is derived from lower chip costs because of reduced per unit area processing costs.

The analysis of the crystal growth process through its various stages from polycrystalline feed stock to polished wafers shows that the advantage of increased crystal diameters is questionable when based strictly on wafer area per unit length of boule or unit weight of polycrystalline feed stock. When made long enough, a float-zone process can be considerably more efficient than a Czochralski process in converting polycrystalline feed to acceptably doped single crystals. Offsetting this advantage are increased wafer thicknesses and kerf losses with large diameter crystals. The principal savings or value derived from using large diameter wafers stems from reduced device processing costs per unit area. Secondarily, the efficiency of utilizing area improves with larger wafer diameters.

The economic impact study was based on substituting 15.2 cm (6 inch) wafers for the currently used 7.6 cm(3 inch) wafers. If one-third of the total number of smaller wafers were replaced by an equivalent area of larger wafers, the annual impact would be about $250-$290 million and a cumulative ten-year impact would be $6.7-$7.3 billion. The use of larger, more complex devices will reduce the cost of finished electronic packages. The economic impact from reduced finished package costs is extremely tenuous; however, based on past experience it could equal the savings derived from reduced chip processing costs.

2.0 INTRODUCTION

There are several advantages that are potentially realizable for a floating-zone crystal growth process carried out under near zero gravity conditions. First, there are the factors that are inherent to a floating zone process whether gravity forces are present or not. One of the principal advantages is that higher purities are possible with containerless crystal growth processes from high temperature melts. Another is the inherently uniform axial dopant levels which result from a zone leveling mode of growth. Second, there are factors arising uniquely as a consequence of the near weightless environment of a space laboratory. One is that buoyancy-induced convection is effectively eliminated from the melt. Lack of control over this transport mechanism is responsible for many common crystallographic defects. Another is that the growth of crystals larger in diameter than can be processed on earth can be entertained because of the absence of the destabilizing effects of gravity forces. The availability of larger crystals can potentially be translated to economic advantage through the value, per se, of large crystal elements or by virtue of higher yields of acceptable crystal chips from the boule.

In order to meet the goal of producing large crystals, it is necessary to overcome the deleterious effects of thermally-induced, residual stresses in the crystal that become emphasized with scale. An ideal solution to this problem is achieved if the conditions of the process are arranged to produce a freezing interface that is a plane perpendicular to the axis of growth.

In a first generation space laboratory for processing large Si crystals, the use of an incandescent heat source is envisioned. This source will heat the melt via radiation and, as the silicon melt is opaque to the emitted radiation, the heating will take place at the surface. In the absence of rotation, heat transport by solid conduction will convey heat to interior regions of the melt but this mechanism is inadequate for large diameter crystals.

Rotation of the crystal and feed stock provides a means for effecting "in-depth" heating of the melt zone. Rotation also reduces the azimuthal gradients that would exist in the absence of rotation. Relative angular rotational rates between the feed and crystal and/or different crystal and feed stock diameters result in circulating currents within the melt zone and attendant forced convective heat transport. The technological task that presents itself is to define the rotational rates and geometric characteristics of the crystal and feed stock that will result in the circulation currents that are most favorable for producing a stress-free crystal that is also free of crystallographic defects. Although rotation may be used to advantage to induce convective heat transport to the inner regions of the melt, it also results in destabilizing centrifugal forces and can produce periodic variations in the flow field within the

melt zone. The type and degree of rotation must, therefore, be controlled so that the stability limits of the melt are not exceeded and the spatial and temporal variations of velocity associated with the forced circulation currents within the melt are attenuated to the degree necessary to prevent variations in the solute concentration within the growing crystal.

3.0 TECHNICAL INVESTIGATION

3.1 APPROACH

The approach followed in the execution of the technical investigation is outlined below:

- Carry out dimensional analyses to determine order of magnitude influences of the forces and heat transport mechanisms active in the melt zone. Construct the independent dimensionless groups which sets limits on the stability of the melt and characterize the velocity and temperature fields within a stable melt.

- Review the literature relating to the stability of rotating and non-rotating liquid columns. Extend the existing analyses to include an important mode of instability hitherto unreported. Establish the numerical values for the dimensionless groups governing the stability of the melt zone.

- Review the literature relating to the nature of the flow in the melt resulting from rotation. Establish the differential equations which determine the velocity fields in the melt. As the complexity of a complete solution precludes anything but an extensive program involving numerical analysis and computers, carry out simple limiting/type analyses and use the insights provided by the literature dealing with experiments and theory relative to similar flows to gain the best possible understanding of the flow within the molten zone and the important physical factors that influence this flow.

- Establish the differential equations which determine the temperature field within the melt. These equations are relatively easy to solve if the velocity field is established. In lieu of a means for calculating the real velocity field, carry out heat transfer analyses of some simple flow models of the melt to gain understanding of the relative importance of convective and conductive heat transfer mechanisms, temperature distributions, etc.

- On the basis of the preceding, postulate the type of rotation needed to induce the most favorable circulation currents in the melt.

- Suggest necessary and promising avenues for investigation in future work.

3.2 DIMENSIONAL ANALYSIS

Dimensional analysis has been applied to establish the independent dimensionless groups that may govern the behavior of the float-zone process in a near weightless environment in order to: (1) provide order-of-magnitude insight into the relative magnitude of the forces responsible for the absolute stability of the melt zone and the circulation within a stable melt; (2) provide order-of-magnitude insights into the heat transfer mechanisms responsible for the temperature field within a stable melt; and (3) determine the similitude relationships required for scale model experiments.

The technical support for the results follow from a straightforward application of dimensional analysis common to engineering practice. The pertinent results follow.

3.2.1 Nomenclature

a = radius: m

$C_p(T)$ = temperature dependent specific heat of the melt at constant pressure: $j\text{-}Kg^{-1}\text{-}K^{-}$

h = height of the melt zone: m

g = local gravity constant: $N\text{-}Kg^{-1}$

$k(T)$ = temperature dependent thermal conductivity coefficient: $watt\text{-}m^{-1}\text{-}K^{-1}$

L = latent heat of fusion of the melt: $j - Kg^{-1}$

N_B = Bond number: dimensionless

N_{PR} = Prandtl number: dimensionless

N_R = Reynolds number: dimensionless

N_W = Weber number: dimensionless

$q''\left(\lambda, \frac{r}{r_1}, \frac{z}{h}\right)$ = incident radiation from the source as distributed in wavelength and over the melt surface as a function of radius ratio, $\frac{r}{r_1}$, and axial distance ratio, $\frac{z}{h}$: $watt - m^{-2}$

$R\left(\lambda, T, \frac{z}{h}\right)$ = reflection coefficient for the melt as dependent on the wavelength λ of the emitted radiation from the source, the local surface temperature of the melt T, and the angle of incidence of the oncoming radiation expressed as a function of $\frac{z}{h}$: dimensionless

r = radius: m

T = temperature: K

T_o = melting or freezing temperature: K

ΔT = maximum temperature difference between any two radial locations within the melt: K

V = velocity associated with the circulation within the melt: m - sec^{-1}

z = dimension measured in axial direction: m

$\alpha(\lambda, T)$ = absorption coefficient for the melt as dependent on the wavelength λ of the emitted radiation from the source and the local surface temperature T of the melt: dimensionless

β = volume coefficient of expansion of the melt: K^{-1}

$\varepsilon(T)$ = total hemispherical emissivity coefficient (integrated spectral value) as dependent on the local surface temperature T of the melt: dimensionless

γ = Stefan-Boltzmann constant: watt-m^{-2}-K^{-4}

λ = wavelength: m

$\rho(T)$ = temperature dependent density of the melt: Kg-m^{-3}

$\sigma(T)$ = temperature dependent surface tension coefficient: N-m^{-1}

$\mu(T)$ = temperature dependent coefficient of viscosity: Kg-m^{-1}-sec^{-1}

Subscripts:

1 refers to the crystal
2 refers to the feed stock

3.2.2 Application to Stability Requirements

The stability of the melt zone is determined solely by the dimensionless parameters:

- Weber number, $N_W = \dfrac{\rho r_1^3 \omega_1^2}{\sigma}$
- $\dfrac{r_2}{r_1}$
- $\dfrac{h}{r_1}$
- $\dfrac{\omega_2}{\omega_1}$

This result is subject to four restrictions: (1) gravity forces are small in respect to surface tension forces; (2) buoyant forces are small in respect to surface tension forces; (3) viscous forces attendant on the circulation induced in the melt by rotation are small in respect to surface tension forces; and (4) the radial and axial velocities associated with the flow within the melt are small in respect to the peripheral speed of rotation. These restrictions are met if

- Bond number, $N_B = \dfrac{\rho g r_1 h}{\sigma} << 1$
- $\dfrac{\rho g \beta \Delta T r_1^2}{\sigma} << 1$
- $\dfrac{\mu r_1 \omega_1}{\sigma} << 1$
- $\dfrac{V}{r_1 \omega_1} << 1$

Assuming that stability is insured for a Weber number and the geometric ratios $\dfrac{r_2}{r_1}$ and $\dfrac{h}{r_1}$ of the order unity, we will show in following sections that these restrictions are satisfied for Si crystals of large diameter processed in a gravity field appropriate to an earth orbiting space laboratory.

3.2.3 Application to Fluid Circulation Patterns

An incandescent heat source applies no applicable forces of electromagnetic origin to the molten zone. In an operational regime approaching the limits of melt stability, the influence of buoyant and gravity forces have been assessed as unimportant. The effects of variations in the surface tension coefficient on fluid motion are also neglected. Accordingly, the circulation of the melt is determined by inertia and viscous forces and, therefore, the circulation patterns within the melt are determined by:

- Reynolds number, $N_R = \dfrac{\rho r_1^2 \omega_1}{\mu}$
- $\dfrac{r_2}{r_1}$
- $\dfrac{h}{r_1}$
- $\dfrac{\omega_2}{\omega_1}$

3.2.4 Application to the Temperature Field

The temperature field within a stable, axisymmetric melt in vacuo which is opaque to the incident radiation from an incandescent source is determined by:

- Reynolds number, $N_R = \dfrac{\rho r_1^2 \omega_1}{\mu}$
- Prandtl number, $N_{PR} = \dfrac{C_p \mu}{k}$
- $\dfrac{\alpha q'' r_1}{k T_o}$
- $\dfrac{\varepsilon \gamma T_o^3 r_1}{k}$

- $\dfrac{\rho V \, L r_1}{k \, T_o}$
- $\dfrac{r_2}{r_1}$
- $\dfrac{h}{r_1}$
- $\dfrac{\omega_2}{\omega_1}$

2.2.5 Application to Scale Model Tests: A Summary

Similitude in respect to the stability of a melt requires for both the model and prototype that

- $N_W = \dfrac{\rho \, r_1^{\,3} \, \omega_1^{\,2}}{\sigma} = \text{constant}$

(The same value for both model and prototype)

- $N_B = \dfrac{\rho \, g \, r_1^{\,2}}{\sigma} \ll 1$
- $\dfrac{\rho \, g \, \beta \, \Delta T \, r_1^{\,2}}{\sigma} \ll 1$
- $\dfrac{\mu \, r_1 \, \omega_1}{\sigma} \ll 1$
- $\dfrac{V}{r_1 \, \omega_1} \ll 1$
- $\dfrac{r_2}{r_1} = \text{constant}$
- $\dfrac{h}{r_1} = \text{constant}$

- $\dfrac{\omega_2}{\omega_1} = \text{constant}$

Similitude in respect to the velocity field within a stable melt requires for both the model and prototype that

- $N_R = \dfrac{\rho\, r_1^{\,2}\, \omega_1}{\mu} = \text{constant}$
- $\dfrac{r_2}{r_1} = \text{constant}$
- $\dfrac{h}{r_1} = \text{constant}$
- $\dfrac{\omega_2}{\omega_1} = \text{constant}$

Similitude in respect to the temperature field within a stable melt requires for both the model and prototype that

- $\dfrac{\alpha\, q''\, r_1}{k\, T_o} = \text{constant}$
- $\dfrac{\varepsilon\, \gamma\, T_o^{\,3}\, r_o}{k} = \text{constant}$
- $\dfrac{\rho\, V\, L\, r_i}{k\, T_o} = \text{constant}$
- $N_R = \dfrac{\rho\, r_1^{\,2}\, \omega_1}{\mu} = \text{constant}$
- $N_{PR} = \dfrac{C_p\, \mu}{k} = \text{constant}$
- $\dfrac{r_2}{r_1} = \text{constant}$

$$\frac{h}{r_1} = \text{constant}$$

$$\frac{\omega_2}{\omega_1} = \text{constant}$$

3.3 STABILITY ANALYSIS

In our previous work for NASA[(1)*], the absolute stability limits for molten zones of various shapes were discussed in detail but the destabilizing effects of rotation were not a consideration. The results of the previous work are reproduced in Figure 1 which shows the family of zone shapes which obtain under steady pulling conditions in zero gravity. The geometric limit for absolute stability is indicated by the dotted circle. The circle represents the stability limit for a non-rotating system where surface tension forces dominate, and, if exceeded, the molten zone may pinch off into two separate caps.

Hocking[(2)] discusses the case of a rotating cylindrical column of liquid and derives the stability criteria for axisymmetric longitudinal disturbances as well as for disturbances that are the same in all planes perpendicular to the axis of the cylinder that leave the centroid of the perturbed shape on the axis. In the latter case he obtains the curious theoretical result that a region of neutral stability exists in the case of an inviscid liquid which joins the region of instability in case the viscosity is finite. For real liquids his analysis leads to the same condition that we obtained by the simpler means presented in Appendix A, namely that the column is stable if

$$\frac{\sigma}{\rho a^3 \omega^2} > \frac{1}{3}$$

where

$r_1 = r_2 = a =$ radius of zone

$\omega_1 = \omega_2 = \omega =$ angular velocity of zone

In this case the cross section of the molten zone is perturbed to a near elliptical shape; that is, by the lowest order radial disturbance.

Hocking's result for axisymmetric disturbances applies to infinitely long columns of liquid. In the case of columns of finite length, the disturbance must be a standing wave which does not alter the volume of the molten zone so the wavelength must meet the condition

*Superscript numbers in parentheses refer to Section 5.0, REFERENCES

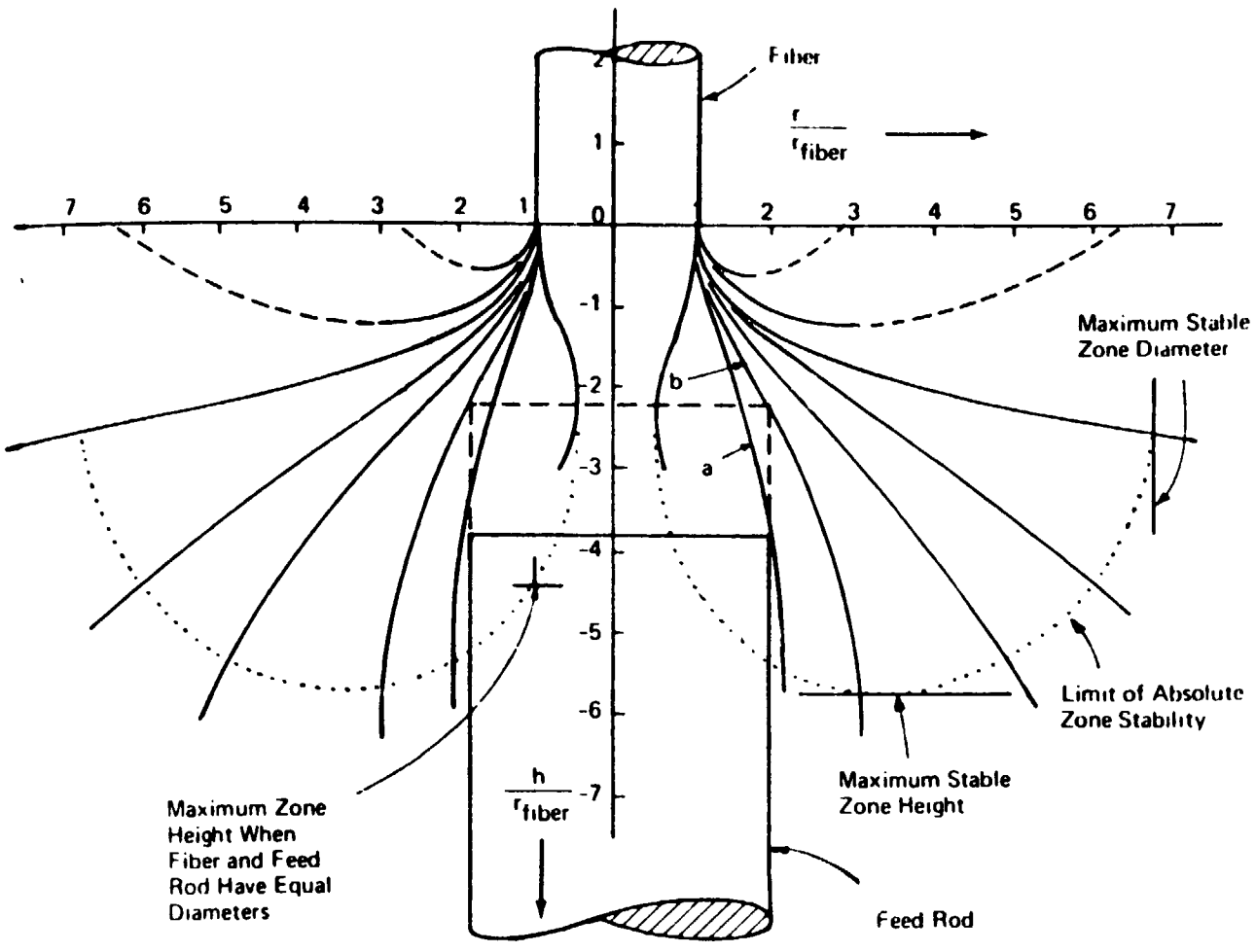

FIGURE 1 **CALCULATED EQUILIBRIUM ZONE SHAPES PLOTTED IN TERMS OF THE ZONE HEIGHT (h) AND RADIUS (r) NORMALIZED TO THE FIBER RADIUS. THE CONTOURS "a" AND "b" REPRESENT POSSIBLE ZONE SHAPES FOR TWO ZONE HEIGHTS BETWEEN THE FIBER AND THE FEED ROD.**

$$n\lambda = h$$

where

n is integer
λ is the wavelength
h is the height of the zone

Then the condition for stability becomes, for n = 1,

$$\frac{\sigma}{\rho a^3 \omega^2} > \frac{1}{4\pi^2 - \left(\frac{h}{a}\right)^2} \left(\frac{h}{a}\right)^2$$

This condition for stability was tested in the experiments of Carruthers and Grasso[3], and they showed it to be applicable over a useful range of their experiments.

In the present program we have examined theoretically the stability of the column with respect to another type of axial distrubance, hitherto unreported in the literature. In this analysis we consider an unsymmetric disturbance corresponding to the condition

$$\frac{1}{2}\lambda = h$$

This is a longer wavelength disturbance than any possible axisymmetric disturbance and must be asymmetric on account of the requirement to preserve the volume of the melt. In this case the molten zone is perturbed to a shape like that of a beam with hinged ends whirling in its first bending mode. In Appendix A the condition for stability is shown to be

$$-\frac{\sigma}{\rho a^3 \omega^2} > \frac{1}{\pi^2}\left(\frac{h}{a}\right)^2$$

Graphs of the two stability limits under conditions of rotation are shown in Figure 2. It is to be noted that the requirement

$$\frac{h}{a} < 2\pi$$

must be met for stability even in the absence of rotation. This is the classical result of Rayleigh and is also indicated by the singularity in Hocking's criterion. Moreover, for absolute stability, as opposed to possible metastable solutions, our previous work set the limit $\frac{h}{a} < 4.3$ for a cylindrical molten zone. However, as Figure 2 shows, the asymmetric disturbance leads to instability for lower rotation rates over the range of h/a of most practical interest.

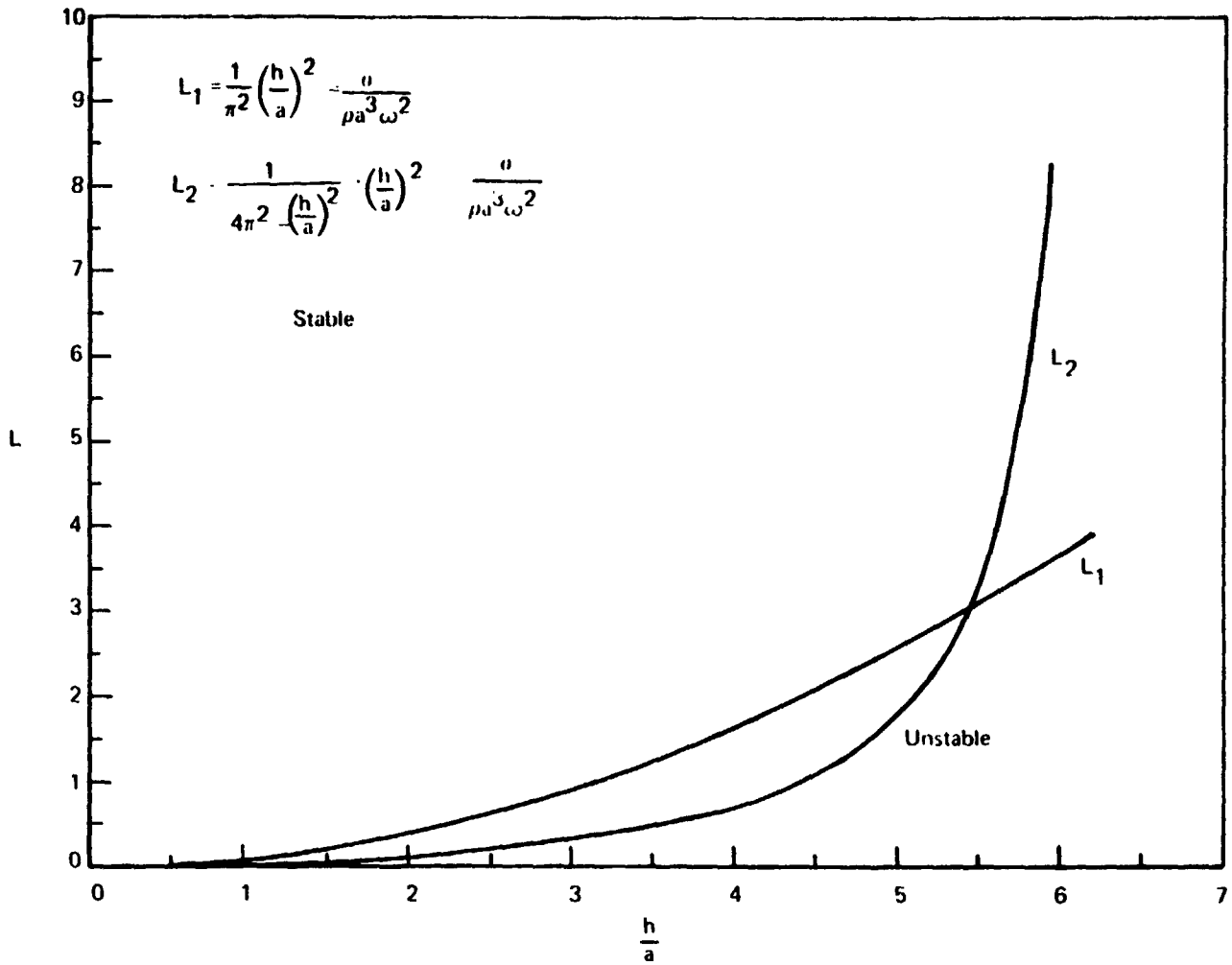

FIGURE 2 GRAPHS OF TWO STABILITY LIMITS

From the above, we might choose a condition of $\frac{h}{a} = \pi$ as a practical working number to satisfy requirements for the in-depth heating of the melt and stability under conditions of rotation. In this case, the least stable limit of those investigated (L_1 of Figure 2) reduces to $\frac{\rho a^3 \omega}{\sigma} = 1$, or a Weber number limit of unity. It is to be noted that these stability analyses, although providing useful quantitative criteria for engineering purposes, are limited. They do not account for the effects of internal circulation within the melt or for a variety of possible ratios of the rotational rates and the radii of crystal and feedstock. To account properly for these effects is a formidable analytical problem. It is a problem where the most efficacious solution is most likely derived from tests. Some suggested experimental methods are described in Section 3.6.

3.4 STABILITY LIMITED MAXIMUM CRYSTAL ROTATION

On the basis of the arguments, limitations, and results presented in Sections 3.2 and 3.3, a calculation of the maximum rotational rate vs. crystal radius has been made for Si molten zones in a radius range of 0.038 m (1.5 in) to 0.304 m (12 in) with results appearing in Table 1. The basis for these calculations are:

$$N_W = \frac{\rho a^3 \omega^2}{\sigma} = 1$$

$$N_B = \frac{\rho g a h}{\sigma}$$

$$r_1 = r_2 = a$$

$$\omega_1 = \omega_2 = \omega$$

$$\frac{h}{a} = \pi$$

$$\sigma = 7.2 \times 10^{-1} \text{ N/m}$$

$$\mu = 2 \times 10^{-3} \text{ Kg/m - sec}$$

$$\rho = 2.2 \times 10^{3} \text{ Kg/m}^3$$

$$g = 9.8 \times 10^{-5} \text{ m/sec}^2 = 10^{-5} \text{ times value at earth's surface}$$

$$\beta \approx 10^{-6}\ K^{-1}$$

$$\Delta T \approx 10^{2}\ K$$

3.5 HEAT TRANSFER AND FLUID FLOW ANALYSIS

3.5.1 General Approach

Heat transfer analysis has two major purposes in application to the float-zone processing of large Si crystals. First, it provides the means to evaluate various design approaches for producing the in-depth heating of the molten zone that is necessary to produce a stress-free crystal and, thereby, best methods may be selected. Second, thermal analysis must be applied to design a process system that is minimized in respect to size, weight and power consumption. In this program thermal analysis is addressed to the first purpose only. Rigorous application to the second purpose follows logically sometime after the practicality of the space processing of large Si crystals is demonstrated to hold real promise. Some estimates of the process system requirements have been made by MSFC, and they are regarded to be consistent with the capabilities of a next generation Sky-Lab.

The ideal conditions of heat transfer to be sought are those that result in a freezing interface that is a plane perpendicular to the axis of growth, for it is this condition that minimizes the thermally induced stresses in the growing crystal. To achieve this ideal requires that the heat flux plus the change of phase heat release per unit area at all local areas of the freezing interface match that transferred to the growing crystal under a unique circumstance; i.e., that the freezing interface is a plane perpendicular to the axis. It is clear that the solution to this problem involves the heat transfer characteristics of the whole system consisting of the polycrystalline feed stock, the molten zone, and the crystal.

Solution to the heat transfer problem associated with the feed stock and crystal is fairly straightforward. As these materials, at their operating temperatures, are opaque to the IR radiation emitted from the molten zone, the solution involves phonon conduction in an axisymmetric system in vacuo with radiation boundary conditions at the exposed cylindrical surfaces* and with either a heat flux or a fixed temperature boundary condition at the ends. We, among others, have developed computer programs to solve this problem routinely.

The difficult problem is the analysis of the heat transfer within the melt. With an opaque melt, we have heat transfer by solid conduction and forced convective heat transfer induced by the rotation of the molten zone. The importance of the heat transport contribution via convection requires that the velocity field within the melt be known, and, more to the point, be manipulated to achieve the desired condition for producing stress-free crystals of uniform composition.

*Other boundary conditions can be easily accommodated.

TABLE 1

PARAMETER LIMITS FOR STABLE, ROTATING, CYLINDRICAL Si MELTS

a	ω	aω	N_R	N_B	$\rho g \beta \Delta T a^2/\sigma$	$\mu a\omega/\sigma$
m	rad/sec	m/sec				
0.038	2.55	0.097	3640	0.0014	4.32×10^{-8}	2.70×10^{-4}
0.076	0.91	0.069	5190	0.0055	1.73×10^{-7}	1.92×10^{-4}
0.152	0.32	0.049	7230	0.0218	6.91×10^{-7}	1.36×10^{-4}
0.304	0.12	0.036	10700	0.0870	2.76×10^{-6}	1.0×10^{-4}

An examination of the last three columns of Table 1 shows that three of the four restrictions necessary to the assumption that inertia and surface tension forces determine stability are satisfied. Satisfaction of the fourth restriction, i.e., $\frac{V}{a\omega} \ll 1$, is questionable. This is discussed in Section 3.5.4 following. The maximum speeds of rotation appearing in Table 1 set the limits within which favorable circulation currents must be sought.

If the influence of temperature on the properties which govern the circulation within the melt be ignored (as we believe it can be), then, the solution to the problem of determining the velocity field within the molten zone can be approached independently of the solution of the thermal problem. In this approach, the material properties which govern the circulation within the melt are fixed at their values measured at the melting temperature. Finally, fluid mechanical considerations applied to the flow within a rotating, stable melt show the flow to take place in the laminar regime which introduces some measure of simplicity in an otherwise very complex problem.

3.5.2 Analysis of Temperature Field within the Molten Zone

The differential equations governing the combined convective and conductive heat transport in a rotating, opaque axisymmetric molten zone circulating in laminar flow are developed in Appendix B. The equation satisfied by the temperature is

$$\left[\frac{\partial^2 T}{\partial r'^2} + \frac{1}{r'}\frac{\partial T'}{\partial r'} + \frac{\partial^2 T'}{\partial z'^2}\right] - \frac{\rho C_p r_1^2 \omega_1}{k}\left[V_r' \frac{\partial T'}{\partial r'} + V_z' \frac{\partial T'}{\partial z'}\right] = 0 \quad (1)$$

where

$$r' = r/r_1$$
$$z' = z/r_1$$
$$T' = T/T_o$$
$$V' = V/r_1 \omega_1$$

subscript

r refers to radial direction
z refers to axial direction

and all other symbols are defined in Section 3.2.1.

The solution to Equation 1 subject to the appropriate boundary conditions (see Appendix B) can be gained by application of numerical techniques and computer calculation provided that the velocity field (V_r' and V_z' as a function of r' and z') are known. The solution is a description of the temperatures in the melt as a function of r' and z', or the temperature field.

It is of some interest to note that the dimensionless coefficient $\frac{\rho C_p r_1^2 \omega}{k}$ is the product of the Reynolds number and the Prandtl number, a result impossible to forecast by dimensional analysis. However, as the Reynolds number is an independent determinant of the velocity field, the Reynolds number and Prandtl number are independent determinants of the temperature field as set forth in Section 3.2.4.

Two factors complicate the solution of Equation 1. F , to be rigorous, the contours of the exposed surface of the molte e under rotating conditions should be known. Second, there i nique solution which specified the isothermal melting and freezing in ce in space coordinates and meets the heat flux boundary conditions at these interfaces. It will require iteration in the computational process in order to determine this unique solution.

The development above was carried out to reveal what is involved in, and methods for, achieving a complete solution to the thermal behavior of the molten zone. Actual solution was beyond the scope of this program.

3.5.3 Evaluation of Azimuthal Temperature Gradients

As shown in Section 3.4, the stability limited maximum allowable rate of crystal and feed-stock rotation varies monotonically from 2.55 rad/sec (24.35 rpm) for a radius of 0.038 m (1.5 in) to 0.12 rad/sec (1.15 rpm) for a radius of 0.304 m (12 in). As a result of concern that such low rotational rates might impose the need for careful control of azimuthal temperature gradients, an analysis of this problem was completed. It was found in all cases that even these low rotational rates result in a considerable reduction (smaller by a factor of 20 to 30) of the temperature gradient that would exist if no rotation were present. The analysis and detailed results appear in Appendix C.

3.5.4 Analysis of Flow Field within the Molten Zone

The problem here is to define the flow field within the molten zone that is most suitable for producing stress-free crystals of uniform composition. A review of the pertinent literature* shows that there are no analytical or experimental results that are adequate to this definition; however, an interpretation of this literature provides useful guidance.

One important simplifying characteristic of the flow field of interest is that it is laminar. Both experiment and theory support this contention. In fact, the literature shows that the Reynold's numbers associated with the fluid currents within the molten zone are of order $\sqrt{N_R}$,

*See REFERENCES

with $N_R \equiv \frac{\rho r_1^2 \omega_1}{\mu}$ as usual. That is, the radial and axial components of the velocities induced in the melt by rotation times the effective hydraulic radius of the current cross sections in local regions is small in respect to the product of the peripheral speed of the crystal, $r_1 \omega_1$, times the crystal radius. As shown in Section 3.4, the maximum value of N_R set by stability for crystal sizes in a range of interest vary from about 3600 to 10,000. Therefore, the Reynolds numbers associated with the radial and axial currents within the molten zone are of order 60 to 100. The experience with steady, incompressible channel flows characterized by Reynolds numbers in this range shows them to be laminar. However, just because the currents flow in the laminar range does not mean they are simple in pattern. In fact, they are very complex. An idea of this complexity is given by the experiments of Hide and Titman[4], Carruthers and Nassau[5] and Carruthers and Grasso[3], even though none of these experiments truly duplicate the conditions imposed on the molten zone in a typical float zone process.

The physical basis for and general character of the flow patterns within the molten zone may be described as follows. Differences in the radii or angular velocity of rotation of either the crystal or feed stock give rise to differences in the radial pressure gradient appearing next to the solid-liquid interfaces resulting from the tangential velocities induced near these surfaces by viscous shear. The differences in the pressure that results near these boundaries at any radius gives rise to axial pressure gradients, and axial flows take place in response to these gradients. The general picture of these flows in an axial plane through its axis of symmetry is one of rising and falling axial flows separated radially by cylindrical surfaces where viscous shear is great and separated axially by radial plane where viscous shear is also large. The flow regions of high shear next to the freezing and melting interfaces are commonly called the Ekman boundary layers. The axial flow next to the outer surface of the melt is called the Rossby layer by Hide and Titman. In cases where the rotational rates of the crystal and feed stock are different, another radial plane of high shear region is located intermediate between the melting and freezing interfaces. Of course, a tangential velocity distribution is present throughout the flow field having local velocities that match those of the crystal and feed stock at the melting and freezing interfaces. The picture in an axial plane, then, is one of rotating cells separated by axial and radial boundary layers. The cells are often called Taylor-Proudman cells in recognition of the pioneering work of these scientists on viscous flows of the type under discussion.

The flow picture described is qualitatively correct but simplified. Depending on the Reynolds number characteristics of the flow, the boundary layers can become large (at low values of Reynolds number) in respect to the linear dimensions of the molten zone and the cellular and boundary layer divisions become smeared. Moreover, at high

Reynolds numbers, shear waves can develop in regions of high viscous shear, as observed by Hide and Titman, which fact further complicates the flow picture.

With the qualitative picture of the behavior of the flow field in mind, the question becomes, how can one select the rotational and dimensional characteristics of the system to best achieve in-depth heating in order to minimize thermal stresses in the growing crystals while obviating variations in solute concentration imparted by flow fluctuations? In simple terms the objective is to convey the heat absorbed at the external surfaces of the melt to interior regions while suppressing temporal and spatial variations in the velocity field.

Figure 3 illustrates in schematic form some more promising arrangements for achieving the desired result. They appear in the order of their expected merits. The expected qualitative features of the fluid flow and heat transfer characteristics of the system shown in Figure 3a is presented below as an example of what might be made to take place in a desirable design.

Starting at a location near the outer surface of the molten zone next to the freezing interface, we note an axial flow directed toward an intermediate radial plane of symmetry where the tangential component of velocity is zero everywhere. This axial stream is heated by the absorbed radiation from the source, and, by virtue of convective heat transport, a major portion of the net radiation absorbed is transferred to the intermediate plane of symmetry. Here the axial stream diverts in direction to flow radially inward in a boundary layer that can be likened to a typical Ekman layer. The radial flow in this boundary layer peels off as it proceeds toward the axis of symmetry giving rise to a uniform axial flow proceeding in the direction of the freezing interface. As this radial flow is bounded by an adiabatic surface at $z = 0$, the temperature of this flow is unchanged. Within the axial flow proceeding from the intermediate plane of symmetry to the freezing interface, we note that the ratio of heat transport by forced convection to solid conduction reduces, becoming zero at the interface. The net effect is that the enthalpy flux entering radially at the intermediate plane, which is nearly the same as the absorbed radiation, is uniformly distributed over the freezing interface where it is released by heat transfer via solid conduction. To complete the picture, the axial flow approaching the freezing interface is diverted to flow radially outward in the Ekman boundary layer next to this interface, thereafter to turn and flow again axially next to the exterior surface of the melt.

In this idealized picture, the intermediate radial plane of symmetry is isothermal wit . temperature elevated above the melting point. The total heat absorbed in the outer layer of the melt is distributed uniformly over the freezing interface. If the crystal is insulated to prevent radial gradients, then, the freezing interface will be a plane perpendicular to the axis of symmetry--the desired result. With the reasonable assumption that the heat flux contribution due to the latent

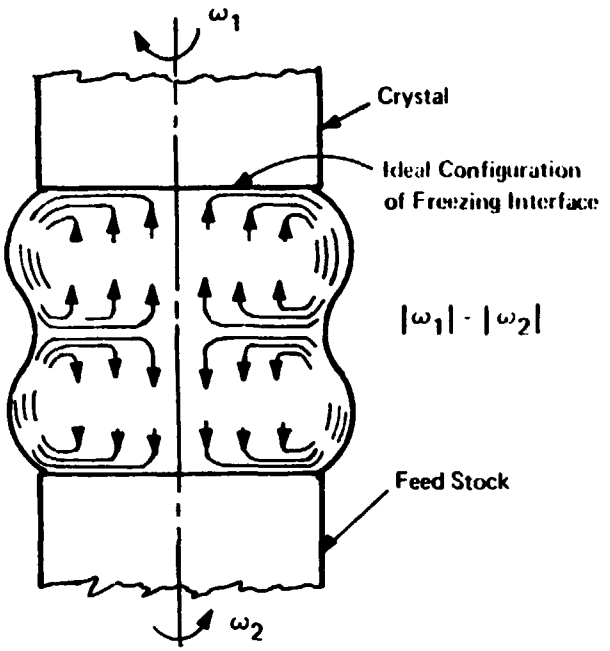

FIGURE 3a

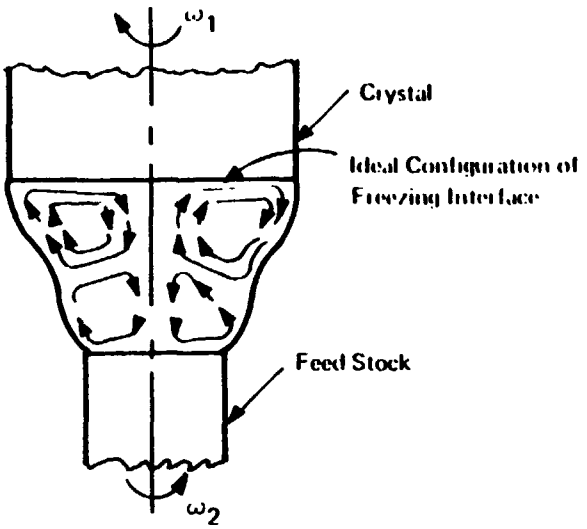

FIGURE 3b

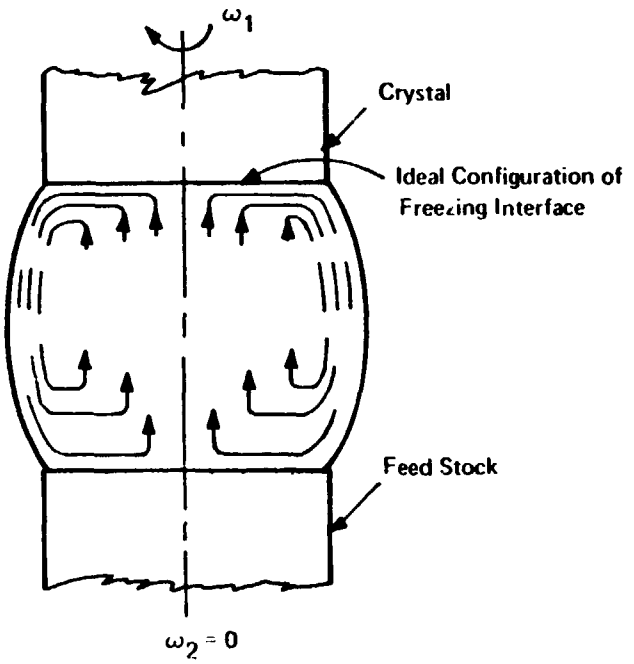

FIGURE 3c

FIGURE 3 SCHEMATIC REPRESENTATION OF AXIAL AND RADIAL COMPONENTS OF VELOCITY FIELD IN MOLTEN ZONE FOR SOME MORE PROMISING FLOAT-ZONE SYSTEMS

heat of solidification is relatively small, the temperature and flow fields in the molten zone between the intermediate plane and the melting interface is symmetrical with respect to those described.

The qualitative nature of the velocity fields associated with the other systems depicted in Figures 3a and 3b can be constructed with reference to that given for Figure 3a. In Figure 3b the path length for solid conduction from the outer surface of the melt to the freezing interface is reduced to take possible advantage of this fact for in-depth heating. Figure 3c is presented as a hedge against the possibility that the location of the intermediate planes that divide the cells in Figures 3a and 3b may fluctuate in space about some mean location, with consequent variations in solute appearing in the growing crystal. The idea advanced here is that the system of Figure 3c is probably more stable in this regard although its heat transport characteristics are less desirable.

The description of the flow field given above borrows heavily from the results of the prior experimenters cited and on the supporting analysis of Hide and Titman. However, it is to be noted that the boundary conditions on the exterior surfaces of the equivalent molten zone in these prior experiments deviate significantly from the real cases of interest in the present investigation.

As a final observation, it is noted that the radial and axial components of velocity within the molten zone as indicated by the measurements of Carruthers et al are small in respect to the peripheral velocity of the crystal. That is, $\frac{V}{a\omega} << 1$, a state satisfying the conditions for the stability criterion advanced in Section 3.4. However, against this, the work of Hide and Titman predict that the radial and axial components of velocity in local regions within the melt can approach the peripheral speed. This being the case, local distortion of the outer surface will result from these local dynamic effects, and the stability criterion might be modified somewhat. Whether these effects on stability are significant is a debatable point. We believe that they are probably not significant, but this contention needs to be tested by experiments of the type proposed in Section 3.6.

An analytical description of the velocity field within the molten zone is provided by the appropriate form of the Navier-Stokes equations together with the equation of continuity. These equations are developed in Appendix D.

For an incompressible, steady, laminar, axisymmetric flow with material properties independent of temperature, the Navier-Stokes equations combined with the continuity equation in dimensionless form are

$$V_r' \frac{\partial V_r'}{\partial r'} - \frac{V_\theta'}{r'} + V_z' \frac{\partial V_r'}{\partial z'} = - \frac{1}{\rho r_1^2 \omega_1^2} \frac{\partial P}{\partial r'}$$

$$+ \frac{\mu}{\rho r_1^2 \omega_1} \left[\frac{\partial^2 V_r'}{\partial r'^2} + \frac{1}{r'} \frac{\partial V_r'}{\partial r'} - \frac{V_r'}{r'^2} + \frac{\partial^2 V_z}{\partial z'^2} \right] \quad (1a)$$

$$V_r' \frac{\partial V_\theta'}{\partial r'} + \frac{V_r' V_\theta'}{r'} + V_z' \frac{\partial V_\theta'}{\partial z'} =$$

$$\frac{\mu}{\rho r_1^2 \omega_1} \left[\frac{\partial^2 V_\theta'}{\partial r'^2} + \frac{1}{r'} \frac{\partial V_\theta'}{\partial r'} - \frac{V_\theta'}{r'^2} + \frac{\partial^2 V_\theta'}{\partial z'^2} \right] \quad (1b)$$

$$V_r' \frac{\partial V_z'}{\partial r'} + V_z' \frac{\partial V_z'}{\partial z'} = - \frac{1}{\rho r_1^2 \omega_1^2} \frac{\partial P}{\partial z'}$$

$$+ \frac{\mu}{\rho r_1^2 \omega_1} \left[\frac{\partial^2 V_z'}{\partial r'^2} + \frac{1}{r'} \frac{\partial V_z'}{\partial r'} + \frac{\partial^2 V_z'}{\partial z'^2} \right] \quad (1c)$$

The equation of continuity alone is

$$\frac{\partial}{\partial r'} \left(r' V_r' \right) + \frac{\partial}{\partial z'} \left(' V_z' \right) = 0 \quad (2)$$

We note here the appearance of the Reynold's number, $\frac{\rho r_1^2 \omega_1}{\mu}$, a result anticipated by the dimensional analysis presented in Section 3.2.3.

Few analytical solutions to Equations 1a-1c and 2 are available. Those that are involve relatively very simple flow systems where the constraints reduce the active variables to manageable proportions. In principle, numerical techniques involving machine computation will serve to achieve a solution for our cases of interest. The introduction of the concepts of a stream function and potential function as an aid to solution does not apply in our case for the potential function does not exist in a system having vorticity, although the stream function exists. Numerical solution to problems of the type we are concerned with utilize

relaxation techniques in both time and space coordinates. The problem statement treats the system in unsteady state (we have to include terms of the form $\frac{\partial V}{\partial t}$) and relaxes it to the steady-state solution employing the appropriate initial and boundary conditions. The paper by Orszag and Israeli[6] reviews the work in this area.

Upon review of the literature pertaining to solution of similar fluid flow problems, one is impressed with the complex nature of possible flows which may result. The work of Pearson[7] on the viscous flow between two rotating coaxial disks having infinite radii makes this point. Even for this relatively simple system which has relatively straightforward characteristic solutions to the Navier-Stokes equations, Pearson shows equilibrium solutions are highly dependent on the Reynolds number based on the disk spacing which is the only geometric dimension in the system. Moreover, the equilibrium solution in some cases, characterizied by a higher Reynolds number, was shown to depend on the start-up condition; that is, which disk is assumed to influence the flow first. This analytical problem is idealized, but the result does give an indication of the sensitivity of the flow pattern to slight variations in the speeds of rotation of the disk.

A determination of the velocity field within the molten zone by numerical solution of the governing equations is outside the scope of the current program. The work presented was carried out with the objective of gaining maximum insight into the nature of flow field short of that provided by computer solution of the governing equations and of defining the magnitude of the problem to be faced should computer solution be attempted.

3.6 FUTURE WORK

In order to pursue the technical investigation beyond what has been accomplished in this program requires: (1) a more accurate determination of the stability of the molten zone under the variety of configurations and rotational rates that may have utility; and (2) a more accurate determination of the velocity field within the molten zones associated with each promising system. Emphasis should be placed on achieving the latter objective.

The work accomplished clearly shows the magnitude of the difficulty associated with a "quantum-jump" in the sophistication of analysis represented by computer solution to the Navier-Stokes equations. Confronted with this difficulty, it would be easy to attempt solutions to problems without adequate knowledge whether the results were warranted or valid. Accordingly, we have concluded that experiments are a vital necessity to the definition of useful flow fields in the Si melt.

Carruthers and Grasso[3] have carried out useful experiments of the type needed. However, these experiments were limited in respect to the stability conditions that they could examine, and the flow patterns that they observed resulted from a boundary condition on the model of the molten zone that was significantly different from that which exist in a real float-zone process.

First, as regards stability, these experiments examined the influence of perturbations which lead to distorted cross sections with a centroid remaining on the axis only. Therefore, they did not examine the effects of the type of perturbation that we have determined to be most limiting as regards the stability of typical melts of interest. Second, these experiments did not examine the influence of internal circulation on stability.

An examination of the Carruthers and Grasso experimental results pertaining to the observed circulation patterns make clear that the experimental method did not produce truly the circulation patterns of a real float zone. This can be seen by reference to the results presented for equal isorotation of equal radii, simulated crystal and feed stock. These results showed significant internal circulations of a magnitude roughly the same as the case of equal counterrotation. From elementary considerations, we know that, in the case of a melt with a free surface, no circulations of the type described can persist at steady state with equal isoration. Anything other than solid body rotation of the complete melt would give rise to shear stresses at the interfaces, a net torque and resulting rate of change in angular momentum of the melt. The induce currents observed by Carruthers and Grasso are the result of shear stresses at the exterior boundary of the simulated melt induced by the mineral oil surroundings. It seems reasonable to assume that the presence of the oil influences the circulation patterns in all the cases they described. To what degree the patterns they observed are different from those of a real float-zone is moot, but their results for equal isorotation make the translation in all cases questionable.

The purpose of experiments we propose in an on-going program would be five fold: (1) they would test the results of the stability analyses that we have made; (2) they would establish stability limits for system configurations and operating conditions not anzlyzed; (3) they would test the validity of concepts we have developed as to the nature of the circulating currents induced in the melt by various forms of rotation; (4) they would provide guidance for the numerical analysis and computer solution of the velocity fields within these melts; and (5) they would obviate some major limitations of prior experiments reported in the literature.

A brief description of the type of experiments we propose is given in Appendix E. The experiments involve the use of scale models and optical tracing of the motion of observable particles suspended in the model melt. From our examination of possibilities, we have found that a model melt system using water with a simulated crystal radius of 2.7×10^{-3} m (0.105 in) has useful potential of meeting the objectives stated above.

4.0 ANALYSIS OF ECONOMIC IMPACT

4.1 SUMMARY

4.1.1 Purpose and Scope

We have considered the possible ten-year economic impact of growing large float-zone silicon crystals in a gravity-free environment. We describe the expected advantages of fabricating large crystals, wafers and chips, and then present examples for the most significant crystal diameters, characteristics and devices.

For this analysis, we have only considered the economic impact on devices that already have a sizable, developed market, and we have assumed replacement of 5 cm (2 inch) float-zone and 7.6 cm (3 inch) Czochralski crystals by 15.2 cm (6 inch) float-zone crystals. We have not conducted an actual volume analysis of specific device types, because the data-gathering and reduction would involve an extensive effort.

The following discussion considers wafer size to be the major influence on the ultimate chip cost. A more extensive analysis will be required to account for the influence of space shuttle costs, power costs in orbit, the practical (rather than theoretical) yield of good crystals, and the actual crystal quality obtainable in a weightless environment.

The conclusions presented in our analysis assume that all of the technical and economic problems of growing and processing 15.2 cm (6 inch) crystals in orbit will be resolved satisfactorily.

4.1.2 Introduction

It appears that crystals several times the present 5-cm (2 inch) and 7.6-cm (3 inch) diameter products currently available could be grown in a gravity-free environment. Large diameter, high quality float-zone crystals would provide a number of economic advantages for manufacturing semiconductor devices. For example:

- The float-zone process produces a greater volume of acceptable dopant level for any given crystal size.
- The float-zone process generally produces higher quality crystals.
- Large float-zone crystals could use large diameter feedstock, which costs less per kilogram than the small diameter feedstock currently used in the float-zone process.

- The large wafers available from large diameter crystals would have much higher efficiencies of surface utilization, which would lead to much greater production of chips per unit area - particularly for large scale integrated circuits.

- The greater number of chips per wafer will greatly reduce the cost per chip, because wafer processing costs are essentially independent of wafer size.

- Large, high quality wafers will enable the production of new, larger classes of rectifiers, thyristors, and LSI's, and these larger, more complex circuits will reduce the overall cost of both finished devices and electronics equipment.

The possibility of growing large float-zone crystals in orbit presents at least one major disadvantage that should be considered:

- The technology necessary to grow large, float-zone crystals in an orbital environment is currently beyond the state of the art, and considerable research and development effort will be required to solve the technical and economic uncertainties inherent in such processing.

4.1.3 Method of Economic Analysis

a. Polycrystalline Feed to Trimmed Boule. As the first step in analyzing the value of large float-zone crystals, we have examined the cost of converting polysilicon feedstock into both Czochralski and float-zone crystals.

We first consider the cost of producing larger diameter feedstock and the possible cost advantage of using such material to produce large float-zone crystals versus smaller Czochralski crystals.

We then consider the cost of producing crystals of equal mass and equal diameter and the value per unit mass of feedstock of the trimmed boules.

Finally, we examine the conversion efficiencies of the two processes, with equal size feedstock, per unit mass of trimmed boule. At this stage, the output of crystal with acceptable dopant level and resistivity determines the value of each trimmed boule.

b. Trimmed Boule to Finished Wafers. The analysis of this manufacturing stage considers wafer output primarily in terms of surface area per unit weight of trimmed boule.

c. Wafer Processing to Finished Chips. This analysis of processing discusses the geometry of area utilization, including the output of chips per unit area as a function of wafer diameter and the influence of larger wafers on area utilization for large chips.

d. Chip Processing Costs. This manufacturing stage is discussed in terms of device complexity (as a function of the number of processing and handling steps), device type and wafer size.

e. Market Impact. Finally, the influence of producing large float-zone crystals in orbit is considered in terms of current and projected market size, device cost as a function of wafer size, and the economic impact on selected device types.

4.1.4 Conclusions

There is no clear-cut cost advantage for either growing process, because there are only marginal savings possible through the different feedstock utilization or conversion efficiencies. In fact, the savings inherent in each process nearly cancel out by the time each type of crystal has been converted to a trimmed boule.

However, it appears that the number of finished chips available from each 15.2 cm (6 inch) wafer could be four to eight times the number of finished chips produced from the currently available 7.6 cm (3 inch) wafers. Therefore, because processing costs are very high and are essentially independent of wafer size, our analysis leads us to conclude that the processing efficiencies made possible by the availability of 15.2 cm (6 inch) wafers would enable the manufacturers of silicon semiconductor devices to produce such devices for perhaps 12% to 25% of the present cost per chip. The theoretical economic impact on the semiconductor industry of such savings can be extrapolated to a cumulative ten-year value of $8 billion to $15 billion.

4.2 CZOCHRALSKI VERSUS FLOAT-ZONE FOR MASSIVE CRYSTALS

4.2.1 Introduction

This section considers the cost of producing crystals from polysilicon feedstock, and examines:

- Feedstock cost as a function of diameter,
- Crystal cost as a function of feedstock size, and
- Conversion efficiency to trimmed boule.

4.2.2 Feedstock Cost

The cost per unit weight of polysilicon feedstock decreases with increasing diameter. This results because radial deposition rates are essentially independent of size and the cost is largely determined by capital and energy costs for the time spent in the trichloro-silane reactor. With these deposition kinetics, the weight of silicon produced per unit time increases proportionally with diameter. Table 2 summarizes the average

TABLE 2

FEEDSTOCK GROWING TIME AND WEIGHT
VERSUS FINAL ROD DIAMETER

Polysilicon Rod Diameter cm(inches)	Length of Deposition Run (days)	Weight of Silicon Per 0.3 m (12") Rod (kg)	Average Production Rate Per 0.3 m (12") Rod (kg/day)
5.7 (2.25)	5.5	1.8	0.33
7.6 (3)	7	3.2	0.46
10.2 (4)	12	5.8	0.48
12.7 (5)	17	8.5	0.50

Source: Arthur D. Little, Inc.

Si production rates as a function of diameter. The average production rate for 12.7-cm (5 inch) polysilicon rod is 50% greater than the rate for 5.7-cm (2.25 inch) rod.

The 7.6-cm (3 inch) Czochralski process currently uses the largest feed rod diameter (12.7 cm, 5 inches), which costs $0.70 to $1.00 per gram, while the 5.7 cm (2.25 inch) float-zone process uses the smallest rod, which cost $1.30 to $1.50 per gram. Thus, for the earth-based process, the float-zone feedstock is 50% more expensive than the Czochralski feedstock, and the latter crystal-growing process enjoys a cost advantage.

4.2.3 Crystal Cost

If both the processes are used to grow 7.6-cm (3 inch) diameter crystals of equal length and equal mass, we find that the Czochralski crystal costs less because of lower feedstock cost. However, we must compare the cost of growing a 7.6-cm (3 inch Czochralski crystal against the cost of growing a 15.2-cm (6 inch) float-zone crystal in orbit--and only consider the growing process itself. Then, we find that both processes use approximately the same diameter feedstock, which would eliminate the feedstock cost advantage of the Czochralski process.

4.2.4 Conversion Efficiency

If 7.6-cm (3 inch) Czochralski crystals are compared with 15.2-cm (6 inch) float-zone crystals, we must consider what percentage of polysilicon is converted by each growth process to the form of a trimmed ingot (or boule) that has been cropped and ground to a specified diameter and length with the desired resistivity for further processing.

Figures 4 and 5 illustrate the geometry of crystal and ingot for the Czochralski and float-zone processes, respectively.

The Czochralski process is used to produce uniform P-type material and both broad-range (2.5:1) and narrow-range (1.7:1) N-type material. When all of the crystal-growing and machining losses and recycling of material have been accounted for, the weight of acceptable P-type trimmed ingot material is about 85% of the initial charge. For the widely used N-type crystals, the material with a broad resistivity range provides about 65% acceptable trimmed ingot, while the narrow-range material provides about 45% of the initial polysilicon charge in the form of usable trimmed ingot. (The charge weight was assumed to be 7.5 kilograms.)

Industry experience with 5.7 cm (2.25 inch) float-zone crystals indicates that a trimmed ingot provides 75-80% acceptable material from a similar initial charge weight (7.5 kg). This compares favorably to the yields of the Czochralski process, depending on the type of crystal grown.

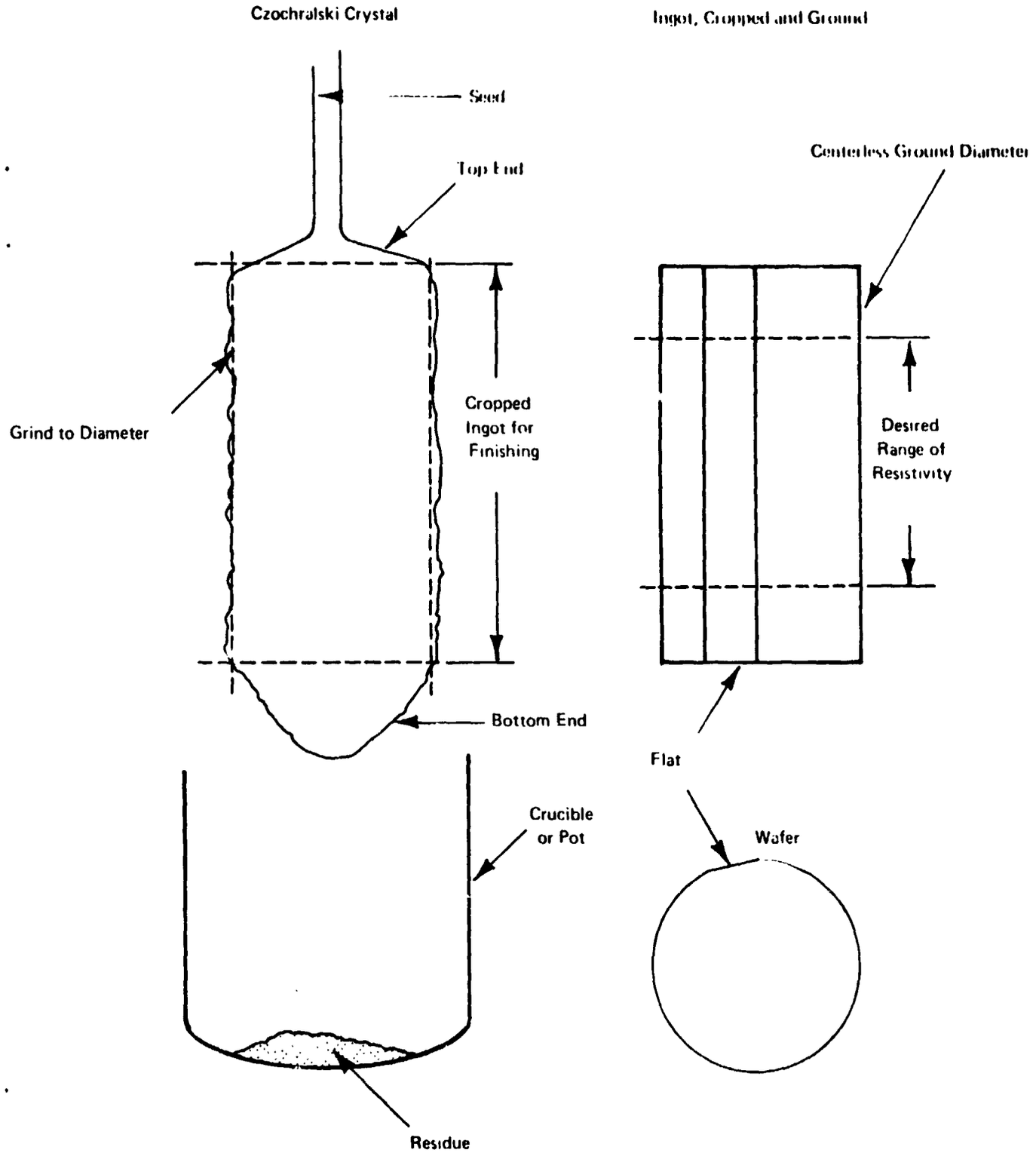

FIGURE 4 GEOMETRY OF CZOCHRALSKI CRYSTAL, INGOT, AND WAFER

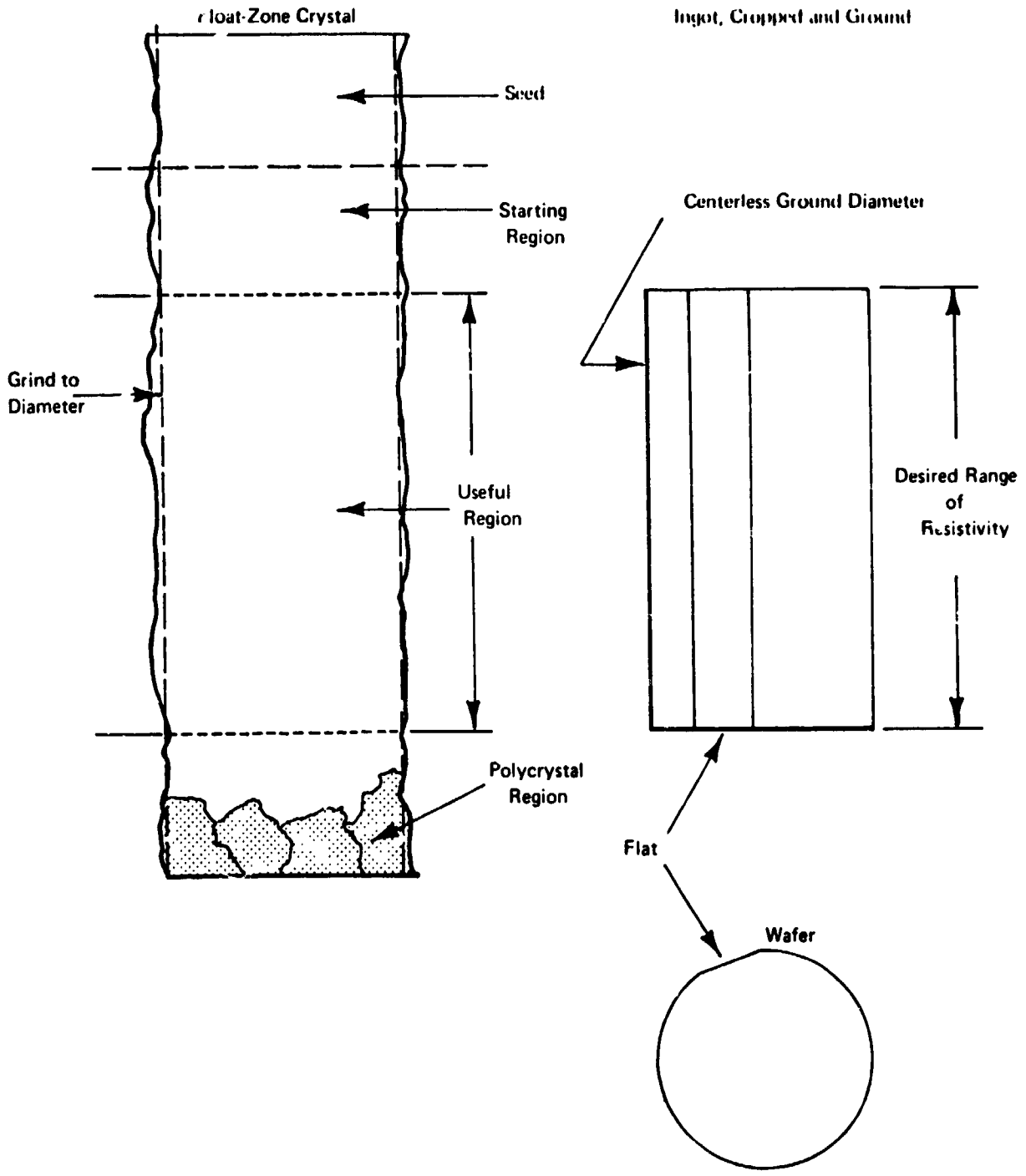

FIGURE 5 GEOMETRY OF FLOAT-ZONE CRYSTAL, INGOT AND WAFER

Because the length of float-zone material lost to ingot cropping may equal two crystal diameters, small charge weights would give unacceptable yields with 15.2-cm(6 inch) diameter crystals. Figure 6 shows the theoretical yield of trimmed ingot available from 7.6-cm (3 inch) and 15.2-cm (6 inch) float-zone crystals, with charge weights ranging from 7 to 100 kilograms. Charges of 50 to 100 kilograms would be required to increase the yield from 15.2-cm (6 inch) crystals to 75-87% acceptable material.

The 15.2-cm (6 inch) float-zone crystal would provide nearly four times the weight of acceptable trimmed ingot per unit length that is available from a 7.6-cm (3 inch) crystal--Czochralski or float-zone.

4.2.5 Conclusions

At this point, it would appear that 15.2-cm (6 inch) float-zone crystals grown in orbit would be perhaps four times as valuable as 7.6-cm (3 inch) Czochralski crystals grown on earth. However, the uncertainties involved with growing the larger crystals in orbit may ultimately negate the theoretical advantage that we have just described. Thus, to this stage in the manufacturing process, neither process has a clear-cut cost advantage. In fact, the average raw material cost is such a small percentage (7-9%) of the cost of a finished device that any savings to this point may have only marginal impact on the ultimate cost of finished chips.

4.3 EFFECTS OF LARGE CRYSTALS ON WAFER FINISHING

Industry experience has shown that the number of wafers per unit length that can be sliced from a trimmed boule decreases with increasing boule diameter. This results in part from the fact that larger diameter wafers must be thicker to survive mechanical handling during finishing and chip processing. Also, saw thicknesses must be increased with larger diameters, which increases kerf losses.

With present technology, approximately eight polished wafers are obtained per centimeter (20 per inch) of trimmed ingot length for 7.6-cm (3 inch) diameter crystals. We have estimated that approximately five wafers per centimeter (12 per inch) could be expected from 15.2-cm (6 inch) crystals. Wafer thickness was increased from .05 to .08 cm (.018 to .030 inch) and saw kerf thickness from .04 to .08 cm (.015 to .030 inch).

Wafer breakage and material losses occur during sawing, lapping, polishing and other wafer finishing procedures. The material losses per unit area should not be influenced significantly by wafer size due to the thicker wafers to be used. We believe that the increased wafer thickness should permit equivalent yields through sawing and lapping (82%) and polishing (85%) steps.

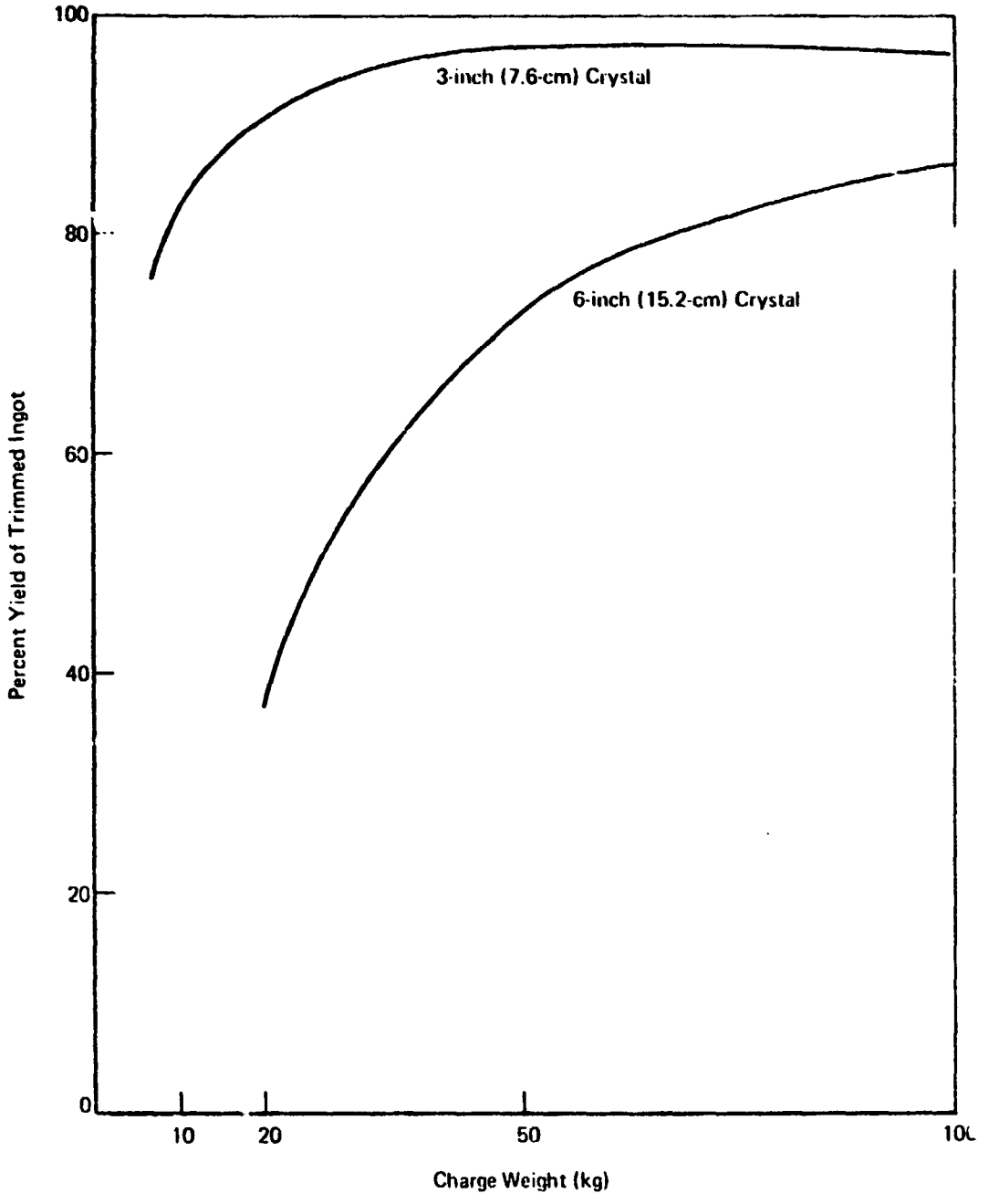

FIGURE 6 THEORETICAL YIELD OF INGOT FROM SINGLE CRYSTALS

Thus, the cost differential between the 7.6-cm (3 inch) diameter wafers and the 15.2 cm (6 inch) diameter wafers is reflected in the wafer area per unit length and area per unit mass of trimmed boule. The larger wafers generate 2.4 times the area per unit length and 0.6 times the area per unit mass of boule. Without specific information about the comparative costs of growing 7.6-cm (3 inch) Czochralski crystals on earth and 15.2-cm (6 inch) float-zone crystals in orbit, it is impossible to make a quantitative estimate of the relative costs per unit area. It is obvious that the larger space-grown crystals will cost more per unit length--probably more than the area differential per unit length. Thus, a cost advantage or value of large wafers will probably be found in reduced device fabrication costs on the larger wafers.

4.4 AREA UTILIZATION BY FINISHED DEVICES

A geometric analysis of the useful area available from both 7.6-cm (3 inch) wafers and 15.2-cm (6 inch) wafers--summarized in Table 3 - indicates that the larger wafer can enclose from five to eight times the number of individual chips than the smaller wafer can. Thus, the value of the larger wafer is even greater than the simple 4:1 ratio of surface areas would suggest.

Two factors make the area converted to chips smaller than the nominal area of the wafer. A rim, usually 0.32 cm (0.125 inch) wide, cannot be used because it is damaged during wafer handling. The percentage of rim area to total area decreases with increasing wafer diameter. Secondly, square or rectangular chips do not fill a circle completely. If any portion of a chip intercepts the outer perimeter, it is unusable. The efficiency of utilizing the enclosed area also improves with increasing wafer diameter. This latter factor is particularly important for the larger chip sizes, which fit inefficiently onto smaller wafers.

4.5 CHIP PROCESSING COSTS

Handling and manufacturing costs for wafer processing have proven to be almost independent of wafer size. Thus, not only does the efficiency of surface utilization increase with wafer diameter, the processing costs per unit area decrease dramatically with larger wafer diameters.

The cost of processing a wafer or producing a finished device is directly related to the device complexity. Figure 7 illustrates the average production cost (including overhead) of wafer processing as a function of complexity, expressed by the number of masks needed to process each wafer.

The linear relationship exists because the major element in the cost per wafer is the labor needed for masking and diffusion transfers. For example, the process for producing Metal-Oxide-Semiconductor (MOS) Large-Scale Integration (LSI) requires nearly 100 transfers of wafers to accomplish the 5 to 7 masking steps. Complex bipolar integrated circuits may require up to twice as much labor cost for handling, transfers, loading of processing

TABLE 3

GEOMETRIC YIELD OF WHOLE CHIPS

Whole Wafer						
Nominal wafer diameter cm-(inches)		5.1 (2)	7.6 (3)	10.2 (4)	12.7(5)	15.2(6)
Useful water diameter (3.2cm, 0.125inch rim)		4.4 (1.75)	7.0 (2.75)	9.5 (3.75)	12.1(4.75)	14.6(5.75)
Useful area (%)		77	84	88	90	92
Square Chips Enclosed in Useful Area						
.635 cm (0.250 inch)	Number of whole chips	24	76	148	256	376
	% Use of nominal area	48	67	74	82	83
1.27 cm (0.500 inch)	Number of whole chips	5	16	32	56	85
	% Use of nominal area	40	56	63	72	75
1.9 cm (0.750 inch)	Number of whole chips	2	6	12	24	32
	% Use of nominal area	36	48	54	59	63
2.5 cm (1.00 inch)	Number of whole chips	0	2	5	8	16
	% Use of nominal area	0	28	40	40	56
Largest Single Chip cm-(inches)		3.1(1.23)	4.9(1.94)	6.7(2.65)	8.5(3.36)	10.3(4.06)
	% Use of nominal area	49	53	56	57	59

Source: Arthur D. Little, Inc.

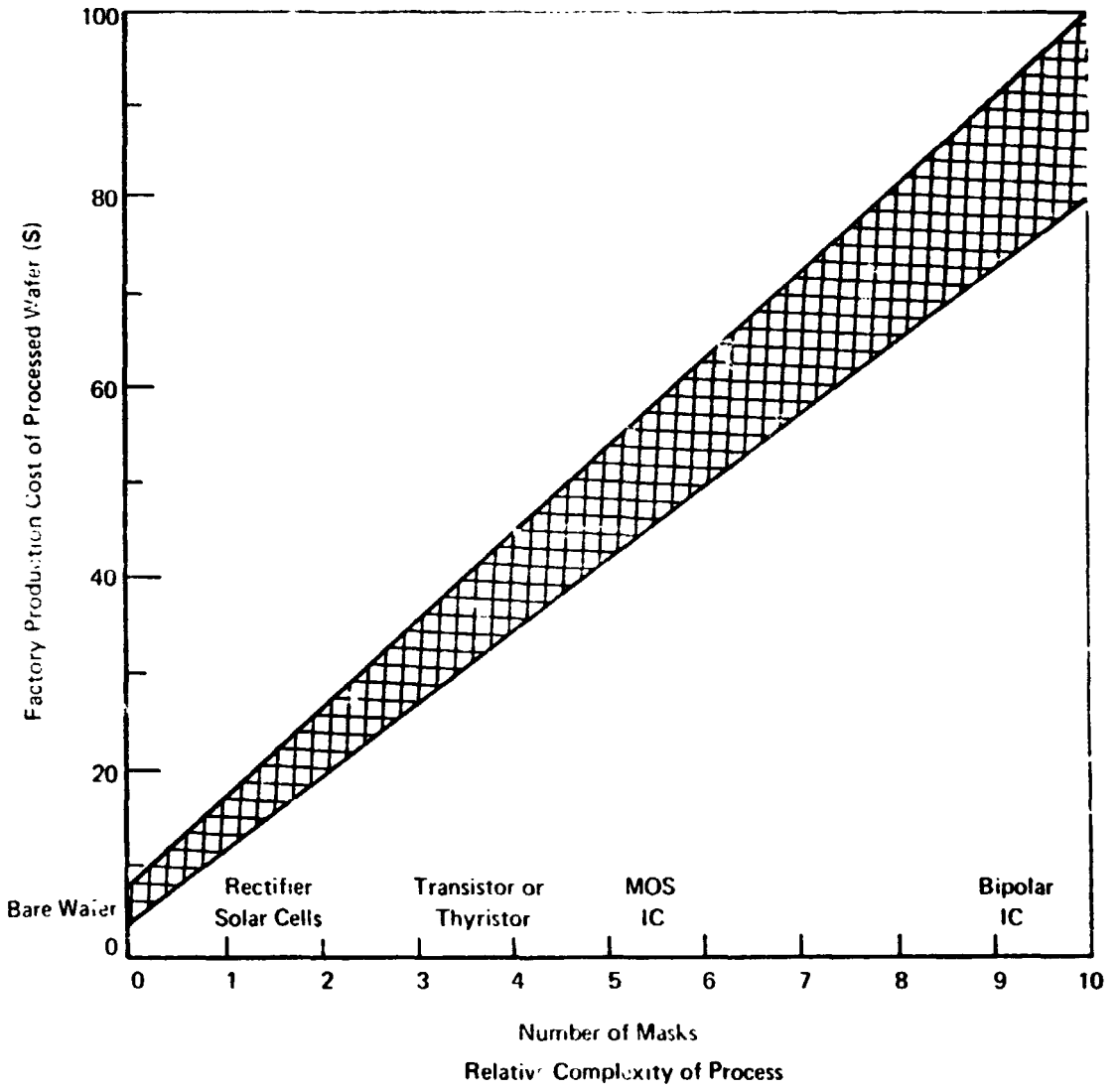

FIGURE 7 COST OF WAFER PROCESSING VERSUS COMPLEXITY OF PROCESS

equipment, inspection and test, because of the 9 to 12 masking steps and other procedures. The labor content ranges from 2.5 to 5 manhours for processing to the point of being cut into individual chips.

As indicated in Figure 7, bare wafers have an average value of approximately $6, while processing costs raise the wafer value to $80 to $100. It is evident that raw material cost is a very small percentage of total finished device cost, except for the most simple devices. The principal savings or value derived from using large diameter wafers stem from reduced processing costs per unit area, because wafer processing costs have historically proven to be essentially independent of size. It is assumed here that wafer processing costs will not increase markedly in going to 15.2 cm (6 inch) diameter Secondarily, the efficiency of utilizing area increases with wafer diameter for the reasons cited in Section 4.4. Thus, the number of chips produced per wafer increases faster than a simple area ratio would predict. The cost of a finished chip produced on the 15.2-cm (6 inch) diameter wafers should be about 1/5 to 1/8 the cost of a chip produced on 7.6-cm (3 inch) diameter wafers.

4.6 MARKET SIZE, GROWTH AND ECONOMIC IMPACT

The 1974 demand for silicon wafers—valued at about $1.00 per square inch (6.5 square cm)—is currently about 200 million square inches (1.3 billion square cm). This demand is growing at an average rate of 20% per year, and therefore is expected to increase sixfold in ten years. Thus, the projected cumulative ten-year market is 25 times the current demand or about 5 billion square inches (32.3 billion square cm)—a market of about $5 billion for raw wafers.

The 1974 production consists of some 40 million wafers and about 60% (or 24 million wafers) were processed to finished devices. At this time, a finished processed wafer represents an average saleable value of approximately $40, so that processing could represent a total annual value of about $1 billion.(A volume analysis for all devices would be necessary to establish the actual value added by processing each year.)

To estimate the theoretical economic impact of substituting 15.2-cm (6 inch) wafers for 7.6-cm (3 inch) wafers, we must assume that the per wafer processing costs remain essentially the same, and that the larger wafers will provide four to eight times the number of finished devices. (Of this also assumes equipment capable of processing the larger wafers, and the hypothesis of equal processing yields.) The annual economic impact of the 15.2-cm (6 inch) wafers could then be 75-88% of $1 billion, or $750-$880 million. In fact, it is only reasonable to consider replacement of about one-third of the smaller wafers with the large diameter wafers. This would lead to an annual impact of about $250-$290 million, and a cumulative ten-year impact of $6.7-$7.3 billion. We believe that the economic impact would be realized primarily through reductions in the price of various finished devices, rather than in the development of a larger market.

An effect, for which there is currently no dollar value, is the possibility of producing much larger, more complex devices on the larger wafers, which will greatly reduce the cost per functi.n in completed systems and thus reduce the overall c st of finished electronic packages. Historically, such impact has shown up as 10-40% reduction in materials and labor costs which are generally 25-35% of finished package costs. At this point, an estimate would be rather tenuous, but it could amount to 2-3% (10%x25%). Considering that production of semiconductor devices supplies an estimated $35 billion in electronic equipment each year, this could result in a savings of $700 million to over $1 billion a year. Long-term results over the decade could ultimately be $15-25 billion.

In actuality, such a theoretical savings can be reached only after considerable research and development to satisfy all technical and economic problems. Currently, all of the crystal growth and wafer finishing procedures assumed in this analysis are beyond the state of the art.

5.0 REFERENCES

1. Arthur D. Little, Inc., Production of Oxide Fibers by a Floating Zone Fiber Drawing Technique, Final Report to NASA Lewis Research Center, NAS 3-13479, February 1971.

2. Hocking, L. M., The Stability of a Rigidly Rotating Column of Liquid, Mathematika, Volume 7, Part 1, June 1960.

3. Carruthers, J. R., and Grasso, M., Studies of Floating Liquid Zones in Simulated Zero Gravity, Journal of Applied Physics, Volume 43, No. 2, February 1972, pp. 436-445.

4. Hide, R. and Titman, C. W., Detached Shear Layers in a Rotating Fluid, J. Fluid Mech. (1967), Volume 29, Part 1, pp. 39-60, Printed in Great Britain.

5. Carruthers, J. R. and Nassau, K., Nonmixing Cells due to Crucible Rotation during Czochralski Crystal Growth, Journal of Applied Physics, Volume 39, No. 11, October 1968, pp. 5205-5214.

6. Orszag, S. A., and Israeli, M., Numerical Simulation of Viscous Incompressible Flows, Annual Review of Fluid Mechanics, Volume 6, (1974), pp. 281-318.

7. Pearson, C. E., Numerical Solutions for the Time-Dependent Viscous Flow between Two Rotating Coaxial Disks, J. Fluid Mech. (1965), Volume 21, Part 4, pp. 623-633, Printed in Great Britain.

6.0 BIBLIOGRAPHY

Batchelor, G. K., Note on a Class of Solutions of the Navier-Stokes Equations Representing Steady Rotationally-Symmetric Flow, Quart. Journ. Mech. and Applied Math., V 1. IV, Pt. 1 (1951), pp. 29-41.

Cisek, T. F., Growth of 40 mm Diameter Silicon Crystals by a Pedestal Technique Using Electric Beam Heating, Journal of Crystal Growth 12 (1972) 281-287 North Hollard Publishing Co.

Noble, J. J., Clomburg, L. A., Hottel, H. C., and Sarofim, A. F., Mathematical and Experimental Modeling of the Circulation Patterns in Glass Melts, Distributed at the Industrial Liaison Symposium, "Heat Transfer," April 22, 1971, pp. 1-12.

Pearson, C. E., A Numerical Study of the Time-Dependent Viscous Flow between Two Rotating Spheres, J. Fluid Mech. (1967) Vol. 28, Part 2, pp. 323-336, Printed in Great Britain.

Proudman, J., On the Motion of Solids in a Liquid Possessing Vorticity, Proc. Roy. Soc. A92, pp. 408-424 (1916).

Stewartson, K., Proc. Camb. Phil. Soc., Vol. 49, pp. 333, 1953.

Taylor, G. I., Experiments on the Motion of Solid Bodies in Rotating Fluids, Proc. Roy. Soc. A104, pp. 213-218 (1923).

Taylor, G. I., Experiments with Rotating Fluids, Proc. Roy. Soc. A100 pp. 114-121 (1921-1922).

Taylor, G. I., Motion of Solids in Fluids, when the Flow is not Irrotational, Proc. Roy. Soc. A93, pp. 99-113 (1916-1917).

Taylor, G. I., The Motion of a Sphere in a Rotating Liquid, Proc. Roy. Soc. A102, 180 (1922).

Taylor, G. I., VII. Stability of a Viscous Liquid Contained between Two Rotating Cylinders, Proc. Roy. Soc. A, Vol. 102, Published February 8, 1923, pp. 289-343.

Wilcox, W. R. and Fullmer, L. D., Turbulent Free Convection in Czochralski Crystal Growth, Journal of Applied Physics, Volume 36, Number 7, pp. 2201-2206.

APPENDIX A

THE STABILITY OF A ROTATING, CYLINDRICAL MOLTEN ZONE

In this appendix we consider the stability of cylindrical molten zone rotating as a solid body. The zone is subjected to two forces: surface tension, which tends to maintain the cylindrical shape, and centrifugal force, which tends to destabilize the zone. We assume that gravity is zero or, at least, negligibly small. The method adopted is to consider a tiny displacement of the equilibrium surface shape and to see whether or not the distortion grows without limit.

First, we consider the distortion to be a function of radium alone. In Figure A1 we show a circle which represents the undistorted cross section of the cylinder with the equation (in polar coordinates)

$$r = a \tag{1}$$

along with a cross section of the distorted cylinder represented by the equation

$$r = a + \epsilon \cos 2\theta \tag{2}$$

The pressure on the undisturbed surface which arises from centrifugal force is

$$p = \omega^2 \rho \int_o^a r\, dr = \frac{\rho \omega^2 a^2}{2} \tag{3}$$

The destabilizing pressure is the change in p due to the change in the shape of the surface and for small changes is given by

$$\Delta p = \rho \omega^2 r \Delta r \tag{4}$$

or

$$\Delta p = \rho \omega^2 a\, \epsilon \cos 2\theta \tag{5}$$

Next we must compute the stabilizing forces produced by the change of curvature of the surface. It is evident from Figure A1 that the greatest curvature of the disturbed surface is at the greatest radius, so the change of curvature does, at least, tend to restore the cross section to circular shape. The change in the other principal curvature also produces a restoring force dependent on the axial height of zone, but we will neglect that in this calculation.

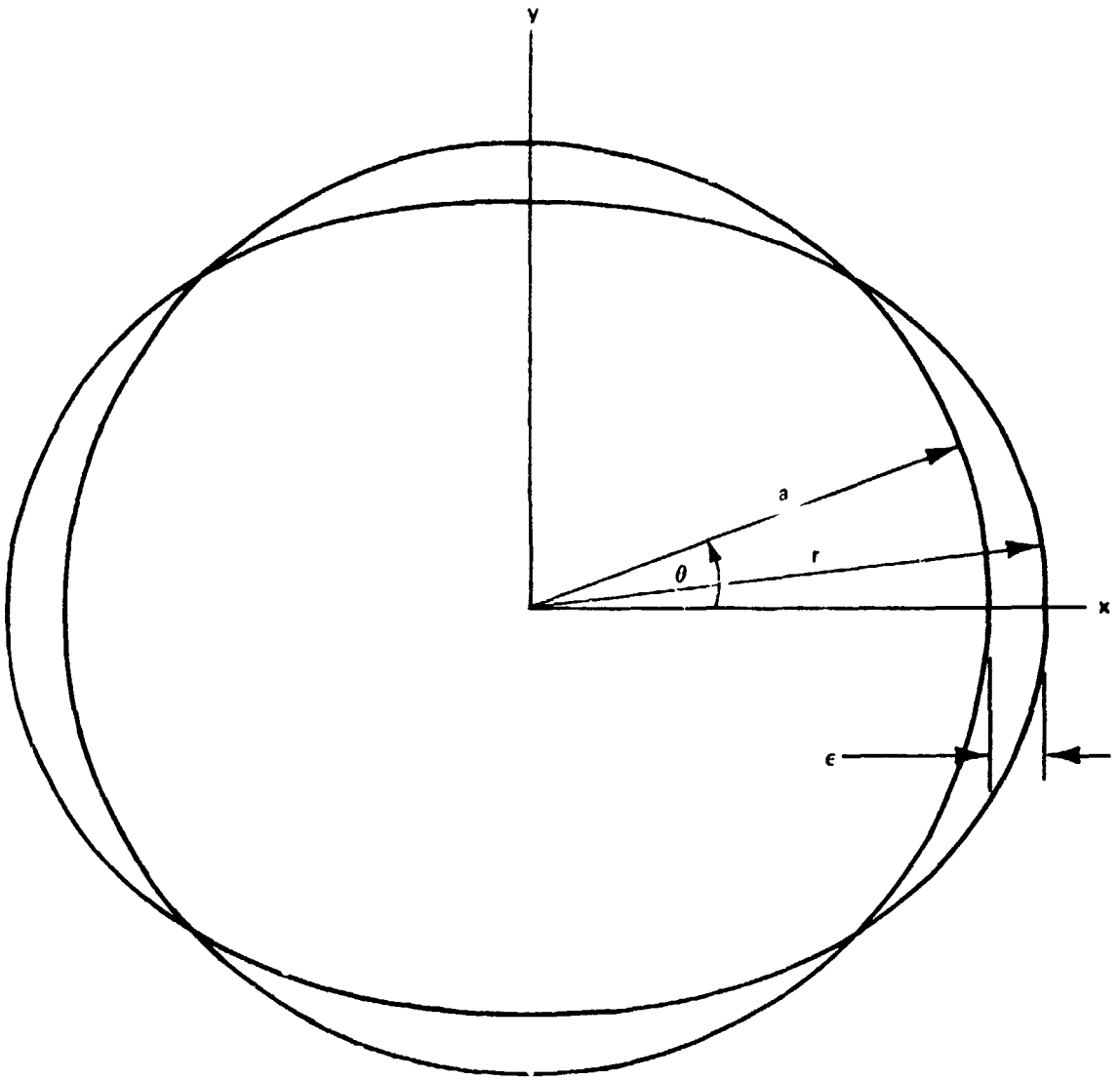

FIGURE A1 CROSS-SECTION OF MOLTEN ZONE IN PERTURBED AND UNPERTURBED STATES

The handiest way to calculate the change in curvature is to use a formula

$$\frac{1}{R} = \frac{r^2 + 2R'^2 - rr''}{(r^2 + r'^2)^{3/2}} \tag{6}$$

that gives the curvature of a curve expressed in polar coordinates, $r = r(\theta)$. Primes denote differentiation with respect to θ. We have

$$\left.\begin{aligned} r &= a + \varepsilon \cos 2\theta \\ r' &= -2\varepsilon \sin 2\theta \\ r'' &= -4\varepsilon \cos 2\theta \end{aligned}\right\} \tag{7}$$

and, to first order,

$$r^2 + 2r'^2 - rr'' = a^2\left(1 + \frac{6\varepsilon}{a}\cos 2\theta\right) \tag{8}$$

$$(r^2 + r'^2)^{3/2} = a^3\left(1 + \frac{3\varepsilon}{a}\cos 2\theta\right) \tag{9}$$

Equations 8 and 9 may be substituted in Equation 6 to give

$$\frac{1}{R} = \frac{a^2\left(1 + \frac{6\varepsilon}{a}\cos 2\theta\right)}{a^3\left(1 + \frac{3\varepsilon}{a}\cos 2\theta\right)} \tag{10}$$

$$\frac{1}{R} = \frac{1}{a}\left(1 + \frac{3\varepsilon}{a}\cos 2\theta\right) \tag{11}$$

whence

$$\Delta\left(\frac{1}{R}\right) = \frac{3\varepsilon}{a^2}\cos 2\theta\ . \tag{12}$$

At the limit of stability

$$\sigma\,\Delta\left(\frac{1}{R}\right) = \Delta p \tag{13}$$

So, from Equations (5) and (12),

$$\frac{3\sigma\epsilon\cos 2\theta}{a^2} = \rho\omega^2 a\,\epsilon\cos 2\theta \tag{14}$$

Thus, to ensure stability, the dimensionless group known as the Weber number must satisfy the inequality:

$$\frac{\rho\omega^2 a^3}{\sigma} < 3 \tag{15}$$

Next, we investigate the situation which occurs when the cylindrical zone of liquid suffers an unsymmetrical displacement in a direction normal to its axis, say in the direction of the x-axis. We take the equation of the disturbed cylinder to be:

$$(x - \epsilon\cos kz)^2 + y^2 = a^2, \tag{16}$$

where $k = \frac{\pi}{h}$

and h is the height of the zone. Figure A2 shows the cylinder with and without the perturbation as well as the system of axes employed.

To first order Equation (16) is

$$x^2 - 2x\epsilon\cos kz + y^2 = a^2 \tag{17}$$

or

$$r^2 - 2a\epsilon\cos kz\cos\theta = a^2 \tag{18}$$

whence we find

$$2r\Delta r = 2a\epsilon\cos kz\cos\theta \tag{19}$$

Equation (19) may be substituted into Equation (4) to give the destabilizing pressure

$$\Delta p = \rho\omega^2 a\epsilon\cos kz\cos\theta \tag{20}$$

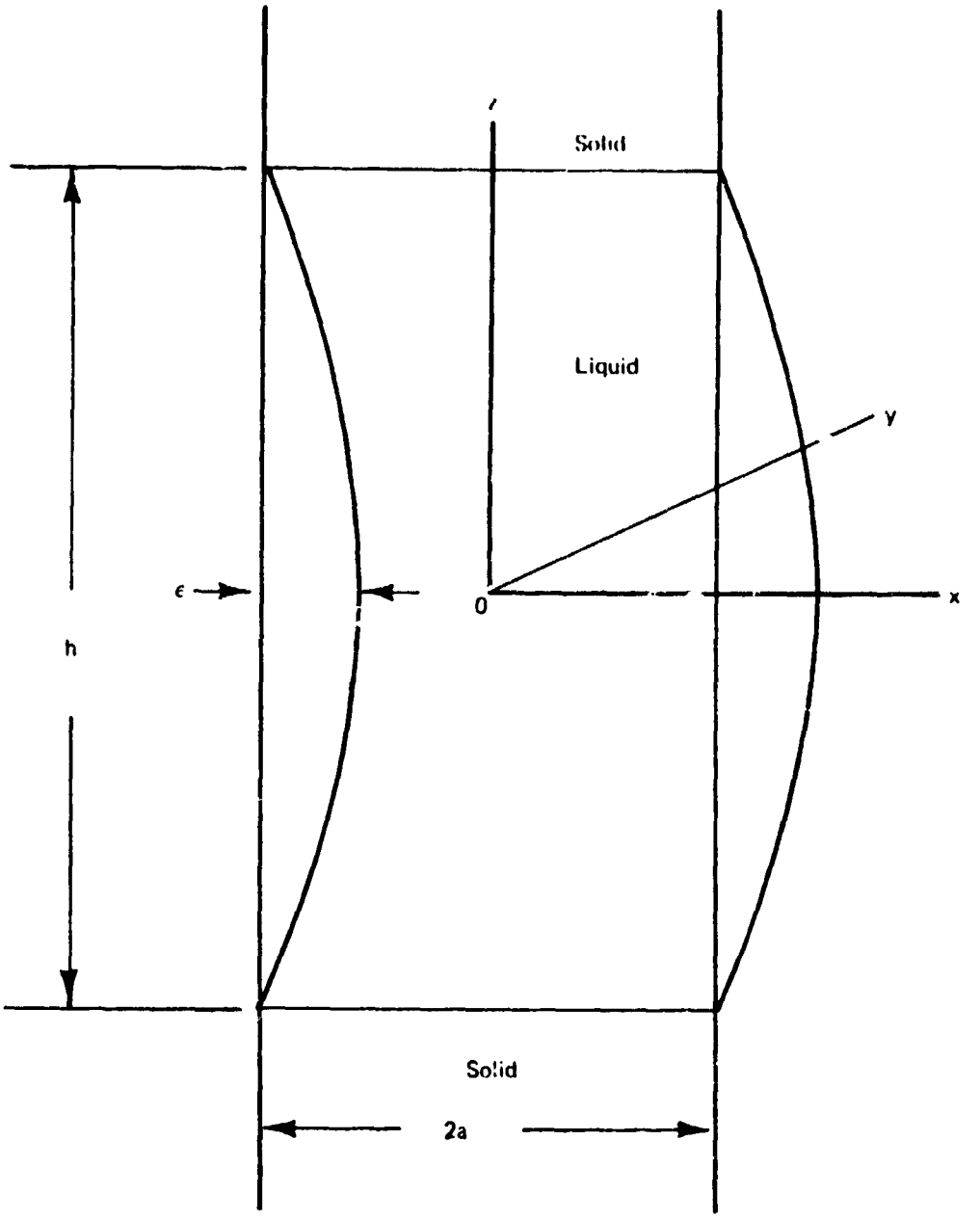

FIGURE A2 CYLINDRICAL MOLTEN ZONE OF RADIUS (a) AND HEIGHT (h), BEFORE AND AFTER PERTURBATION. THE COORDINATE SYSTEM USED IN THE STABILITY ANALYSIS IS ALSO SHOWN.

As before, the stabilizing pressure is obtained after calculating the change in curvature. In this case, we consider the curvature in a plane passing through the z-axis

$$\frac{1}{R} = \frac{-\frac{\partial^2 r}{\partial z^2}}{\left[1 + \left(\frac{\partial r}{\partial z}\right)^2\right]^{3/2}} \tag{21}$$

From Equation (18), we find

$$\frac{\partial r}{\partial z} = - k \varepsilon \sin kz \cos \theta \tag{22}$$

$$\frac{\partial^2 r}{\partial z^2} = - k^2 \varepsilon \cos kz \cos \theta \tag{23}$$

so,

$$\frac{1}{R} = k^2 \varepsilon \cos kz \cos \theta \tag{24}$$

Since this curvature is zero in the case of the unperturbed cylinder, the right hand size of Equation (24) is the change in curvature which gives rise to a stabilizing pressure due surface tension. We have, for the limit of stability

$$\sigma k^2 \varepsilon \cos kz \cos \theta = \rho \omega^2 a \varepsilon \cos kz \cos \theta \tag{25}$$

and hence we obtain the stability criterion for the height of the rotating cylindrical melt in terms of the Weber number as follows:

$$\frac{\rho \omega^2 a h^2}{\sigma} < \pi^2 \tag{26}$$

or

$$\frac{\rho \omega^2 a^3}{\sigma} < \pi^2 \left(\frac{a}{h}\right)^2 \tag{27}$$

APPENDIX B

EQUATIONS GOVERNING THE TEMPERATURE FIELD WITHIN THE MOLTEN ZONE

The purpose of this appendix is to set forth the equations governing the combined convective and conductive heat transport in a melt circulating in laminar flow. Appropriately cylindrical coordinates are chosen (r, θ, z) with:

V_r, V_θ, V_z = velocity components

k = thermal conductivity

q" = rate of heat generation per unit volume

T = temperature

t = time

ρ = density

μ = viscosity

The basic differential equation governing the thermal behavior of the molten zone results from application of the energy equation to an elemental volume of dimensions dr, rdθ, dz. For material properties assumed independent of temperature, the equation satisfied by the temperature is

$$k\left[\frac{1}{r}\frac{\partial}{\partial r}\left(r\frac{\partial T}{\partial r}\right)+\frac{1}{r^2}\frac{\partial^2 T}{\partial \theta^2}+\frac{\partial^2 T}{\partial z^2}\right]-\frac{\rho Cp}{r}\left[\frac{\partial}{\partial r}(r V_r T)+\frac{\partial}{\partial \theta}(V_\theta T)+\frac{\partial}{\partial z}(r V_z T)\right]$$

$$+ q''' \rho Cp \frac{\partial T}{\partial t} \ldots \qquad (1)$$

For the axisymmetric case, with an opaque melt at steady state, Equation (1) reduces to

$$\left[\frac{1}{r}\frac{\partial}{\partial r}\left(r\frac{\partial T}{\partial r}\right)+\frac{\partial^2 T}{\partial z^2}\right]-\frac{\rho Cp}{rk}\left[\frac{\partial}{\partial z}(r V_r T)+\frac{\partial}{\partial z}(r V_z T)\right] = 0 \qquad (2)$$

or alternately,

$$\left[\frac{\partial^2 T}{\partial r^2} + \frac{1}{r}\frac{\partial T}{\partial r} + \frac{\partial^2 T}{\partial z^2}\right] - \frac{\rho Cp}{k}\left[T\frac{\partial V_r}{\partial r} + V_r\frac{\partial T}{\partial r} + \frac{V_r T}{r} + V_z\frac{\partial T}{\partial z} + T\frac{\partial V_z}{\partial z}\right] = 0 \quad (2b)$$

Introducing the condition for continuity of matter

$$\frac{\partial}{\partial r}(r V_r) + \frac{\partial}{\partial z}(r V_z) = 0 \quad (3)$$

reduces Equation (2b) to

$$\left[\frac{\partial^2 T}{\partial r^2} + \frac{1}{r}\frac{dT}{dr} + \frac{\partial^2 T}{\partial z^2}\right] - \frac{\rho c}{k}\left[V_r\frac{\partial T}{\partial r} + V_z\frac{\partial T}{\partial z}\right] = 0 \quad (4)$$

By substituting the non-dimensional variables

$$r' = \frac{r}{r_1}$$

$$z' = \frac{z}{r_1}$$

$$T' = \frac{T}{T_o}$$

$$V_r' = \frac{V_r}{r_1\,\omega_1}$$

$$V_z' = \frac{V_z}{r_1\,\omega_1}$$

where

r_1 = radius of crystal

T_o = melting or freezing temperature

ω_1 = angular velocity of rotation of crystal

Equation (4) becomes

$$\left[\frac{\partial^2 T'}{\partial r'^2} + \frac{1}{r'}\frac{\partial T'}{\partial r'} + \frac{\partial^2 T'}{\partial z'^2}\right] - \frac{\rho C p r^2 \omega_1}{k}\left[V_r' \frac{\partial T'}{\partial r'} + V_z' \frac{\partial T'}{\partial z'}\right] = 0 \quad (5)$$

The boundary conditions for the molten zone are

$$\alpha q_n'' - \varepsilon \sigma T^4 = -k\left(\frac{\partial T}{\partial r}\sin\theta + \frac{\partial T}{\partial z}\cos\theta\right) \quad (6)$$

for the exposed surface of the melt, and

$$-k\frac{\partial T}{\partial z}\Big|_2 \cos\theta = -k\frac{\partial T}{\partial z}\Big|_1 \cos\theta + L u \rho \quad (7)$$

$$\frac{\partial T}{\partial r}\Big|_1 = \frac{\partial T}{\partial r}\Big|_2 \quad (8)$$

$$T_1 = T_2 = T = T_o \quad (9)$$

for the freezing interface, and

$$k\frac{\partial T}{\partial z}\Big|_2 \cos\theta = k\frac{\partial T}{\partial z}\Big|_1 \cos\theta + L u \rho \left(\frac{r_1}{r_2}\right)^2 \quad (10)$$

$$\frac{\partial T}{\partial r}\Big|_1 = \frac{\partial T}{\partial r}\Big|_2 \quad (11)$$

$$T_1 = T_2 = T = T_o \quad (12)$$

where

q_n'' = the oncoming radiant heat flux per unit area normal to the surface of the molten zone.

θ = angle between the outward directed normal to the bounding surface and the positive z direction.

u = rate of crystal growth or pulling rate.

r_2 = radius of feed stock

ω_2 = angular velocity of rotation of feed stock.

subscript 1 refers to the melt side of the interface

2 refers to the crystal or polycrystal side of the interface

The solution to Equation (5) subject to the boundary conditions (6) through (12) can be gained by application of numerical techniques and computer calculation provided that the velocity field (V_r' and V_z' as a function of r' and z') are known. The solution is a description of the temperatures in the melt as a function of r' and z', or the temperature field.

APPENDIX C

REDUCTION OF AZIMUTHAL TEMPERATURE GRADIENTS BY ROTATION

We consider the silicon crystal, the molten zone and the feed rod to be a long cylinder which is rotating as a solid body. We assume that the cylinder is subject to surface heating which is not uniform in azimuth and ask what effect rotation has in reducing the azimuthal temperature gradient thus produced.

The equation satisfied by the temperature T in steady state is

$$\nabla \cdot k\nabla T - C_p \rho v \nabla T = 0 \qquad (1)$$

where

k is thermal conductivity, watts cm^{-1} K^{-1}

C_p is heat capacity, joules g^{-1} K^{-1}

ρ is density, g cm^{-3}

v is velocity vector, cm sec^{-1}

The velocity is in the θ-direction only and has the component

$$V_\theta = \omega r \qquad (2)$$

where

ω is the angular velocity, radians sec^{-1}

r is the radius, cm

Next, we assume the properties of the material to be constant and write Equation 1 in cylindrical coordinates:

$$\frac{k}{r}\frac{\partial}{\partial r}\left(r\frac{\partial T}{\partial r}\right) + \frac{k}{r^2}\frac{\partial^2 T}{\partial \theta^2} - C_p \rho \omega \frac{\partial T}{\partial \theta} = 0 \qquad (3)$$

It seems simplest to adopt an indirect procedure at this juncture in the study of the azimuthal gradient problem. We assume a suitable form for the temperature distribution and derive the heat input from it by computing the radial gradient at the surface. We let

$$T = y(r)\, e^{i\theta} \qquad (4)$$

and substitute this expression in Equation 3 to find the function y(r) which gives the dependence of temperature on the radius. After the substitution is made and some obvious algebraic manipulations are performed, Equation 3 reduces to a form of Bessel's equation:

$$r \frac{d}{dr}\left(r \frac{dy}{dr}\right) - \left(1 + \frac{i\, C_p \rho \omega}{k} r^2\right) v = 0 \qquad (5)$$

The solution is seen to be

$$y = - T_o J_1 (\sqrt{-i}\, Kr), \qquad (6)$$

where

$$K = \sqrt{\frac{C_p \rho \omega}{k}} \qquad (7)$$

and T_o is an arbitrary constant (degrees C) which relates to the amplitude of the gradient.

The Bessel function of complex argument appearing in Equation 6 is customarily expressed in terms of Kelvin functions. We find the temperature distribution to be

$$T = T_o(ber_1 Kr + i\, bei_1 Kr)\, e^{i\theta} \qquad (8)$$

The radial heat flux q" (watts cm^{-2}) is given by the formula

$$q'' = - k \frac{\partial T}{\partial r}\Big|_a \qquad (9)$$

where a is the radius of the cylinder, cm.

From Equation 8 we see that

$$q'' = - k\, T_c \left\{\frac{1 - i}{\sqrt{2}} K(ber_o Ka + i\, bei_o Ka) + \frac{1}{a}(ber_1 Ka + i\, bei_1 Ka)\right\} \qquad (10)$$

It is useful to consider the magnitude of the ratio of the surface temperature, T_a, to the heat flux. From Equations 10 and 8, it may be seen that

$$\left|\frac{T_a}{q''}\right| = \frac{1}{Kk}\sqrt{\frac{ber_1^2\,Ka + bei_1^2\,Ka}{\left(\frac{ber_o Ka + bei_o Ka}{\sqrt{2}} + \frac{ber_1 Ka}{Ka}\right)^2 + \left(\frac{bei_o Ka - ber_o Ka}{\sqrt{2}} + \frac{bei_1 Ka}{Ka}\right)^2}} \tag{11}$$

For short we let the radical appearing in Equation 11 be called u(Ka), which function is tabulated in Table C1. For small values of Ka, the function is seen to be equal to its argument. For large values of Ka, one could appeal to the known properties of the Kelvin functions to evaluate u(Ka), but it is easier to return to Equation 5 and obtain an approximation directly.

First we make the transformation

$$z = r^{\frac{1}{2}} y \tag{12}$$

in Equation 5 to obtain the equation for z:

$$\frac{d^2 z}{dr^2} - \left(\frac{3}{4r^2} + iK^2\right) z = 0 \tag{13}$$

For large values of Kr we may drop the term $3z/4r^2$ in Equation 13 to obtain the simpler equation

$$\frac{d^2 z}{dr^2} - iK^2 z = 0 \tag{14}$$

whose solution is readily seen to be

$$z = A\, e^{\frac{1+i}{\sqrt{2}} Kr} \tag{15}$$

where A is an arbitrary constant. Therefore, the temperature T is given by the formula

$$T = \frac{A}{\sqrt{r}} e^{\frac{1+i}{\sqrt{2}} Kr + i\theta} \tag{16}$$

TABLE C1

Function to be Used in Determining Azimuthal Temperature Gradients

Ka	u(Ka)
0.0	0.00000
0.5	0.49871
1.0	0.96090
1.5	1.26132
2.0	1.33012
2.5	1.27218
3.0	1.19586
3.5	1.13960
4.0	1.10576
4.5	1.08689
5.0	1.07595

$$q'' = \frac{KAk}{\sqrt{a}} e^{\frac{1+i}{\sqrt{2}}Ka+i0} \left(\frac{1+i}{\sqrt{2}} - \frac{1}{2Ka}\right) \tag{17}$$

The magnitude of the ratio of surface temperature to heat flux is thus found to be

$$\left|\frac{T_a}{q''}\right| = \frac{1}{Kk\sqrt{1 - \frac{1}{\sqrt{2}Ka}}} \simeq \frac{1}{Kk\left(1 - \frac{1}{2\sqrt{2Ka}}\right)} \tag{18}$$

to first order.

While the results we have derived so far are useful to predict the azimuthal temperature gradient to be expected when the azimuthal distribution of heat flux is known or can be estimated, it may be of more value in the preliminary stages of system design to consider the ratio of the temperature gradient which appears in the absence of rotation to the gradient obtained with rotation in the presence of the same azimuthal distribution of heat flux. This ratio, which we call the smoothing factor f, is given by the relation

$$f = \frac{K\,a}{u(Ka)} \tag{19}$$

For large values of Ka the smoothing factor is given by the approximate formula

$$f = Ka - \frac{1}{2\sqrt{2}} \tag{20}$$

For values of Ka > 4, this approximation produces less than 1% error. In Table C2 are shown the values of the smoothing factor f for Ka $\leq$ 5.

In order to evaluate Ka, we use the following values to describe the physical properties of silicon:

$$k = 0.22 \quad cm^{-1}\,K^{-1}$$

$$\rho = 2.2\ g\ cm^{-3}$$

$$\sigma = 720 \times 10^{-5}\ N\ cm^{-1}$$

$$C_p = 1.044\ J\ g^{-1}\,K^{-1}$$

and we use the Weber number, given by the ratio

$$N_w = \frac{\rho a^3 \omega^2}{\sigma} \tag{21}$$

to determine the rotation rate ω. Combining Equations 21 and 7, we may write

$$Ka = \left(\frac{C_p}{k}\right)^{\frac{1}{2}} (\sigma \rho N_w a)^{\frac{1}{4}} \tag{22}$$

Finally, we take $N_w = 1$ and find from Equation 22 that

$$Ka = 13.7429\, a^{\frac{1}{4}} \quad (a \text{ in cm}) \tag{23}$$

For a > 1 cm, it is clear that the smoothing factor can be taken roughly to be equal to Ka. Some values of the smoothing factor f and corresponding rotation rates as a function of crystal radius a are shown in Table C3. In spite of the low rotation speeds, the smoothing factors are all quite large, a fact which may be attributed to the rather low thermal conductivity of the silicon near its melting temperature.

TABLE C2

S oothing Factor

a	f
0.0	1.0000
0.5	1.0026
1.0	1.0407
1.5	1.1892
2.0	1.5036
2.5	1.9651
3.0	2.5087
3.5	3.0713
4.0	3.6174
4.5	4.1403
5.0	4.6471

TABLE C3

Smoothing Factors and Rotational Rates for a Weber Number of Unity

a, cm	f	rpm
5	20	15.5
10	24	5.5
15	27	3.0
20	29	1.9
25	30	1.38
30	32	1.05

APPENDIX D

EQUATIONS GOVERNING THE FLOW FIELD WITHIN THE MOLTEN ZONE

In this appendix we set forth the equations governing the circulation of the melt in laminar flow. They are the Navier-Stokes equations and the equation of continuity appearing widely in the literature. Appropriately, a cylindrical coordinate system (r, θ, z) is chosen with

V_r, V_θ, V_z = velocity components

ρ = density

μ = viscosity

Axial symmetry, incompressibility and steady state is dictated. Gravity forces and variations in material properties with temperature are assumed to be negligible. Under these conditions, the Navier-Stokes equation combined with the continuity equation, is

$$\rho\left(V_r \frac{\partial V_r}{\partial r} - \frac{V_\theta^2}{r} + V_z \frac{\partial V_r}{\partial z}\right) = -\frac{\partial P}{\partial r} + \mu\left[\frac{\partial^2 V_r}{\partial r^2} + \frac{1}{r}\frac{\partial V_r}{\partial r} - \frac{V_r}{r^2} + \frac{\partial^2 V_r}{\partial z^2}\right] \quad (1a)$$

$$\rho\left(V_r \frac{\partial V_\theta}{\partial r} + \frac{V_r V_\theta}{r} + V_z \frac{\partial V_\theta}{\partial z}\right) = \mu\left[\frac{\partial^2 V_\theta}{\partial r^2} + \frac{1}{r}\frac{\partial V_\theta}{\partial r} - \frac{V_\theta}{r^2} + \frac{\partial^2 V_\theta}{\partial z^2}\right] \quad (1b)$$

$$\rho\left(V_r \frac{\partial V_z}{\partial r} + V_z \frac{\partial V_z}{\partial z}\right) = -\frac{\partial P}{\partial z} + \mu\left[\frac{\partial^2 V_z}{\partial r^2} + \frac{1}{r}\frac{\partial V_z}{\partial r} + \frac{\partial^2 V_z}{\partial z^2}\right] \quad (1c)$$

The continuity equation alone is

$$\frac{\partial}{\partial r}(rV_r) + \frac{\partial}{\partial z}(rV_z) = 0 \quad (2)$$

With the substitution of

$$r' = \frac{r}{r_1}$$

$$z' = \frac{z}{r_1}$$

$$V_r' = \frac{V_z}{r_1 \omega_1}$$

$$V_z' = \frac{V_z}{r_1 \omega_1}$$

$$V_\theta' = \frac{V_\theta}{r_1 \omega_1}$$

Equations 1a through 2 assume the non-dimensional forms

$$V_r' \frac{\partial V_r'}{\partial r'} - \frac{V_\theta'}{r'} + V_z' \frac{\partial V_r'}{\partial z'} = - \frac{1}{\rho r_1^2 \omega_1^2} \frac{\partial P}{\partial r'}$$

$$+ \frac{\mu}{\rho r_1^2 \omega_1} \left[\frac{\partial^2 V_r'}{\partial r'^2} + \frac{1}{r'} \frac{\partial V_r'}{\partial r'} - \frac{V_r'}{r'^2} + \frac{\partial^2 V_z'}{\partial z'^2} \right] \qquad (3a)$$

$$V_r' \frac{\partial V_\theta'}{\partial r'} + \frac{V_r' V_\theta'}{r'} + V_z' \frac{\partial V_\theta'}{\partial z'} =$$

$$\frac{\mu}{\rho r_1^2 \omega_1} \left[\frac{\partial^2 V_\theta'}{\partial r'^2} + \frac{1}{r'} \frac{\partial V_\theta'}{\partial r'} - \frac{V_\theta'}{r'^2} + \frac{\partial^2 V_\theta'}{\partial z'^2} \right] \qquad (3b)$$

$$V_r' \frac{\partial V_z'}{\partial r'} + V_z' \frac{\partial V_z'}{\partial z'} = - \frac{1}{\rho r_1^2 \omega_1^2} \frac{\partial P}{\partial z'} +$$

$$\frac{\mu}{\rho r_1^2 \omega_1} \left[\frac{\partial^2 V_z'}{\partial r'^2} + \frac{1}{r'} \frac{\partial V_z'}{\partial r'} + \frac{\partial^2 V_z'}{\partial z'^2} \right] \qquad (3c)$$

$$\frac{\partial}{\partial r'} \left(r' V_r' \right) + \frac{\partial}{\partial z'} \left(r' V_z' \right) = 0 \qquad (4)$$

We note here the existence of the Reynolds number, $\frac{\rho r_1^2 \omega_1}{\mu}$, a result anticipated by the dimensional analysis presented in Section 3.2.

Few analytical solutions to Equations 2 and 3a-3c are available. Those that are involve relatively very simple flow systems where the constraints reduce the active variables to manageable proportions. In principle, numerical techniques involving computer computation will serve to achieve a solution for our cases of interest. The introduction of the concepts of a stream function and potential function as an aid to solution does not apply in our case for the potential function does not exist in a system having vorticity, although the stream function exists. Numerical solution to problems of the type we are concerned with utilize relaxation techniques in both time and space coordinates. The problem statement treats the system in unsteady state (we have to include terms of the form $\frac{\partial V}{\partial t}$) and relaxes it to the steady-state solution employing the appropriate initial and boundary conditions. In our case, the initial conditions would be $V_r = V_\theta = V_z = 0$ everywhere except at the boundaries.

The boundary conditions are:

At the cylindrical surface, r = f(z)

$$P = \sigma\left(\frac{1}{R_1} + \frac{1}{R_2}\right)$$

where:

P = static pressure

σ = the coefficient of surface tension

R_1 and R_2 = the principal radii of curvature of the surface of the melt zone under conditions of insured stability.

At the boundary z = 0 (assumed plane)

$$V_r = V_z = 0$$

$$V_\theta = r\,\omega_1$$

At the boundary z = h (assumed plane)

$$V_r = V_z = 0$$

$$V_\theta = r\,\omega_2$$

APPENDIX E

SOME PROPOSED EXPERIMENTS

In order to model the behavior of a stable Si melt in the spacecraft environment, we should ideally produce an earth-based test system in which the inertial forces due rotation are about equal to the surface tension forces and each is large in respect to gravity forces. This means that the dimensions of the model melt must be relatively very small. Backing off from the ideal, we might establish tentatively the condition that the inertia, surface tension and gravity forces are all the same magnitude in the model melt. This would establish a reasonable upper bound on the size and the magnitude of the circulating currents that we can expect to produce in the laboratory.

For the reasons stated above, our model melt should meet, as a minimum, the conditions:

$$N_W = \text{Weber No.} = \frac{\rho a^3 \omega^2}{\sigma} = 1 \qquad (1)$$

$$N_B = \text{Bond No.} = \frac{\rho g a^2}{\sigma} = 1 \qquad (2)$$

$$\frac{h}{a} = 1$$

$$N_R = \text{Reynolds No.} = \frac{\rho a^2 \omega}{\mu} \text{ as large as possible} \qquad (3)$$

To meet the condition expressed by the limiting value of the Bond number, we wish to select a fluid substance that has the smallest possible ratio of ρ/σ in order to experiment with a model having the largest possible dimensions. The Weber number limit for stability coupled with the desire for a model melt having the largest possible dimensions also dictates the selection of a fluid having a minimum value of ρ/σ. The desire for a large Reynolds number, on the other hand, calls for a large value of ρ and a small value of μ. On expressing the Reynolds number in terms of the Weber number, we get

$$N_R = \sqrt{N_W a \rho \sigma}\ /\mu$$

and with $N_W = 1$

$$N_R = \sqrt{a \rho \sigma}\ /\mu$$

As a result of investigation into substances that might best meet the conditions above and are, in addition, readily available, easy to use, and best be transparent for flow visualization studies, we find that water appears as a good candidate. For water at room conditions:

$$\rho = 1 \times 10^{3} \text{ Kg/m}^{3} = 1 \text{ gm/cm}^{3}$$

$$\sigma = 7.2 \times 10^{-2} \text{ N/m} = 72 \text{ dyne/cm}$$

$$\mu = 1 \text{ cm.} = 1 \times 10^{-3} \text{ Kg/m-sec}$$

$$a = \sqrt{N_B \frac{\sigma}{\rho g}} = \sqrt{(1) \frac{\sigma}{\rho g}} = 2.71 \times 10^{-3} \text{ m}$$

$$N_R = \sqrt{a \rho \sigma} / \mu = 441$$

$$\omega = \frac{N_R \mu}{\rho a^2} = 60 \text{ rad/sec} = 573 \text{ rpm}$$

A Reynolds number of 400 is down by a factor of about ten from those values that can be achieved in stable Si molten zones in a space-based process. Examination has revealed that a model system with mercury makes possible experiments at a maximum Reynolds number of 2300. Stability and gravity limits restrict the radius of the mercury model to some value less than about 0.19 cm, and certainly flow visualization studies with mercury will be less rewarding.

However, from what we know now, it is not clear at what value of Reynolds number the optimum benefits from rotation is to be achieved. One view contends that the optimum lies with larger Reynolds numbers. This view is based on the assumption that the character of the flow would have a certain similarity independent of Reynolds number in the Reynolds number range of interest. The assumption of the more circulation the better may still be true, but as the entire character of the flow may well change in the Reynolds number range of interest, this simple assumption is in question. In fact, flows characterized by larger Reynolds numbers may have shear waves and other undesirable periodic features. It seems more reasonable, in the light of our current knowledge, to consider utilizing better defined and understood flows even though they may not represent the optimum that might eventually be achieved. In this light, experiments with water still appear to be very useful.

☆U.S. GOVERNMENT PRINTING OFFICE 1975-641-255/1 REGION NO. 4